Optical Transmitter for Ultra-Wide Band Signals

Rodrigo Silva Maciel
Faculdade de Ciências
Universidade do Porto

A dissertation submitted for the degree of
Master in Physical Engineering

Porto 2012

Jury:

President	Prof. António Manuel Pais Pereira Leite
External Examiner	Prof. Luís Filipe Mesquita Nero Moreira Alves
Supervisor	Prof. Henrique Manuel C. F. Salgado
Co-supervisor	Prof. José A. Machado da Silva

"Let the future tell the truth and evaluate each one according to his work and accomplishments. The present is theirs; the future, for which I have really worked, is mine."

Nikola Tesla

Acknowledgements

First, I would like to thank my parents, Alípio and Gracinda, and my girlfriend Tânia for their invaluable support and patience throughout the time I have been enrolled with this work.

I would also like to thank my supervisors, Prof. Henrique Salgado and Prof. José Machado da Silva, for their priceless help in the technical field without which this work would have been much harder to complete.

I also wish to thank everybody who has been with me during this time at INESC TEC - UTM, namely Dr. Luís Pessoa, Dr. João Oliveira, Mário Pereira and Nuno Sousa for all the important and productive discussions about this project. Thanks also to Nuno Sousa for providing me the Matlab files necessary for running the VCSEL's simulations.

Without you all, this work would not have been possible.

Abstract

In this work, the design of an optical transmitter for Ultra-Wide Band (UWB) signals in the 3.168-3.696 GHz frequency range is presented. Two different approaches have been addressed in this work. First, a discrete low-noise amplifier based on commercial off-the-shelf components (COTS) is described. An application-specific design of an integrated circuit is also discussed. This has been achieved using a combination of electronic design automation (EDA) software. The MOS process used in the integration stage is an IBM 130 nm, a suitable process for the desired application.

An introduction to the motivations for designing such a transmitter as well as the need for the use of such wide band signals is presented. UWB is a wireless technology offering high data-rates and providing noise-like signals. However, it has a short range which can be extended through the use of fiber technology. The goal of this work concerns the design of a suitable electro-optic converter for UWB-over-fiber systems. As such, radio-over-fiber technology is presented and UWB is also discussed. Theoretical descriptions are made throughout, including the diode laser dynamic operation models and the techniques used to design both versions of the transmitter based on the desired performance. Specific issues at each different design stage are also addressed.

These techniques are then applied to the design of the optical transmitter, allowing one to obtain most of its properties in order to assess its performance under real-life scenarios. An estimated maximum range of 31 meters is found for the discrete version, in combination with a high gain and low overall noise figure. The integrated circuit also presents these features and it is, as intended, capable of delivering a small dimension and simple structure device suitable for a wide range of applications.

Resumo

Neste trabalho é apresentado o projecto de um transmissor óptico para sinais de banda ultra-larga (UWB) na gama de frequências de 3.168 - 3.696 GHz. Foram projectadas duas versões diferentes deste transmissor. Primeiro é descrito um amplificador de baixo ruído baseado em componentes discretos e comerciais. Depois, é discutida a implementação de uma versão em circuito integrado. Estes dispositivos foram projectados usando uma combinação de software EDA. Na integração o processo MOS utilizado é o IBM 130 nm, pois apresenta as características apropriadas para o uso pretendido.

É apresentada uma introdução às motivações de implementar um transmissor óptico e a necessidade de utilizar tais sinais de banda larga. UWB é uma tecnologia sem fios que permite grandes taxas de transferência de dados e com um comportamento semelhante a ruído. No entanto, apresenta um curto alcance que pode ser aumentado utilizando fibras ópticas. O objectivo deste trabalho prende-se com o projecto de um conversor electro-óptico capaz de ser utilizado em sistemas UWB-sobre-fibra. Assim, a tecnologia rádio-sobre-fibra é discutida bem como as características dos sinais UWB. Diversas descrições teóricas são feitas ao longo deste trabalho, incluindo os modelos de funcionamento dinâmico dos díodos laser e as técnicas utilizadas para projectar cada uma das versões deste transmissor baseadas nas características desejadas. Desafios particulares relativos ao projecto de cada versão também são discutidos.

Estas técnicas são depois aplicadas ao projecto do transmissor óptico, permitindo obter as suas propriedades de forma a avaliar o seu comportamento em situações reais. Um alcance máximo de 31 metros foi estimado para o dispositivo com componentes discretos, bem como um alto ganho e uma figura de ruído total baixa. O circuito integrado também apresenta estas características e é, como pretendido, capaz de originar um dispositivo final de pequenas dimensões e estrutura simples, adequado para um vasto leque de aplicações.

Contents

1 Introduction **1**

1.1 Background and Motivation 1

1.2 Thesis Organization 3

1.3 Contributions 3

2 Electro-Optic Converter for RoF Applications **5**

2.1 Introduction 5

2.2 Optical Systems for RF Signal Transmission (Radio-over-Fiber) . . . 5

2.3 UWB Signals 7

2.4 VCSEL 9

2.4.1 Structure and Properties 9

2.4.2 Model 10

2.4.3 Small Signal VCSEL Response 12

2.4.4 Relative Intensity Noise 13

2.5 Summary 14

3 Design of RF Amplifiers **16**

3.1 Introduction 16

3.2 Techniques for Designing Discrete RF Amplifiers 16

3.3 Integration Using a MOS Process 21

3.3.1 Analogue Microelectronics Theory 21

3.4 Summary 24

4 Design of the Optical Transmitter for a 3.168-3.696 GHz UWB Signal **25**

4.1 Introduction 25

4.2 General Structure of the Transmitter 26

4.3 Properties of the Amplifier 26

4.3.1 Frequency Stability 26

4.3.2 Gain . . . 28
4.3.3 Noise Figure . . . 29
4.4 Transistors' Biasing Network Design . . . 29
4.5 VCSEL Biasing Network Design . . . 31
4.6 Design of the Impedance Matching Circuits . . . 33
4.7 MOS Process . . . 35
4.8 Design of the IC Transmitter . . . 35
4.9 Summary . . . 37

5 Implementation and Simulation of the Optical Transmitter 39
5.1 Introduction . . . 39
5.2 Implementation in ADS™ . . . 40
5.3 ADS™ Simulation Results . . . 41
5.3.1 S-Parameters . . . 41
5.3.2 Noise Figure . . . 43
5.3.3 Non-Linear Distortion . . . 44
5.3.4 Error Vector Magnitude (EVM) . . . 46
5.4 Integration using the IBM 130 nm MOS Process with Cadence™ . . . 49
5.5 Cadence™ Simulation Results . . . 50
5.5.1 S-Parameters . . . 50
5.5.2 Noise Figure . . . 51
5.5.3 Non-Linear Distortion . . . 52
5.6 Layout of the Integrated Circuit using Cadence™ . . . 53
5.7 Summary . . . 56

6 Conclusion 57

References 59

A Power Relation Between Spurious and Fundamental Components Through Intermodulation Distortion 62

B Free-Space Path Loss 64

List of Figures

1.1 Typical setup of an optical transmitter for UWB signals in Radio-over-Fiber systems. 2

2.1 General scheme of a RoF system [1]. 6
2.2 Band structure of UWB spectrum. 8
2.3 General VCSEL structure, indicating the active region's length (L_a) [2]. 9
2.4 VCSEL equivalent circuit of the laser parasitics. 12
2.5 Small signal transfer function of the VCSEL. 13

3.1 Schematic diagram of a 2-port network. 17
3.2 Diagram of a typical amplifier, including a transistor and its corresponding source and load matching circuits. 18
3.3 Matching circuit using stubs: L is the length of the stub and d is its length position along the transmission line. 20
3.4 Microstrip line model: d is the thickness of the substrate with ϵ_r permittivity and W is the width of the line [3]. 20
3.5 Small-signal equivalent circuit model of a FET when considering the channel-length modulation effect and some intrinsic capacitances. . . 22
3.6 Input impedance matching scheme used. 23
3.7 Bondpad and bonding wire model. 23

4.1 General scheme of the transmitter to be designed. 26
4.2 Stability circles for the amplifier at 4 GHz with the used reflection coefficients. 27
4.3 Scheme of the biasing network used to bias both transistors (T_1 and T_2 are the $\lambda/4$ transmission lines). 30
4.4 Biasing network for the VCSEL. 32
4.5 Frequency response of the VCSEL biasing circuit and parasitics. . . . 33
4.6 Schematic representation of an implemented matching network using a short-circuited stub. 33

4.7 Simplification made to the matching networks between the first and the second transistor. 34

5.1 Schematic of the LNA and the VCSEL biasing circuit in ADS™. . . . 40
5.2 Magnitude and phase of the S_{21} and S_{11} parameters of the LNA. . . . 43
5.3 Simulated noise figure of the LNA. 44
5.4 Linear (red) and compression curve (blue) of the LNA. 45
5.5 UWB signal spectra after several transmission stages for an input power of -30 dBm. 46
5.6 Simulation setup used for the EVM simulations. 47
5.7 Transmitter EVM results for different input power values. 48
5.8 Constellation diagrams of the UWB signal after passing through the optical transmitter, using different input powers. 48
5.9 Schematic of the circuit used for simulations, made with Cadence™. . 49
5.10 Magnitude and phase of the S_{21} parameter and magnitude of the S_{11} parameter of the circuit implemented with Cadence™. 51
5.11 Noise figure of the LNA. 52
5.12 Compression curve and 1 dB compression point of the LNA. 53
5.13 Layout of the components making the IC. 54
5.14 One of the transistors designed, where the stacked layout technique can be observed. 55

A.1 Input-to-output power characteristics of a non-linear system. 62

List of Tables

2.1 Different modulation schemes and coding rates used for obtaining the several data rates defined for UWB signals [4]. 8
2.2 Laser parameters used. 11
2.3 Values of the parasitic components. 12

4.1 Values of the components used in the biasing network. 30
4.2 Values of the components of the VCSEL biasing network. 32
4.3 Dimensions of the transmission lines (TL) and stubs (S) used in the matching networks 1, 2 and 3 of figure 4.1. For example, the length of the first line of the matching network 2, $TL_{2,1}$, is 143.5 mil. 35
4.4 Values of the components of the IC biasing network. 36
4.5 Values of the electrical components used for the VCSEL biasing network in the IC. 37

5.1 UWB signal parameters chosen for simulation purposes. 41
5.2 Third-order intercept points and SFDR of the transmitter. 44
5.3 1 dB compression points. 45
5.4 Input and output-referred third-order intercept points for the circuit implemented using Cadence™. 52
5.5 Input and output-referred 1 dB compression points for the circuit implemented using Cadence™. 53

List of Acronyms

ADS™	Advanced Design System™
BER	Bit Error Rate
BS	Base Station
BSs	Base Stations
COTS	Commercial Off-the-Shelf
CS	Central Station
DC	Direct Current
DCM	Dual Carrier Modulation
EVM	Error Vector Magnitude
FEC	Forward Error Correction
FET	Field-Effect Transistor
IC	Integrated Circuit
IIP3	Input-referred Third-order Intercept Point
ILD	Intrinsic Laser Diode
IMD	Intermodulation Distortion
IO	Input-to-Output
LNA	Low-Noise Amplifier
MOS	Metal-Oxide-Semiconductor
OFDM	Orthogonal Frequency Division Multiplexing
OIP3	Output-referred Third-order Intercept Point
PCB	Printed Circuit Board
Q Factor	Quality Factor
QPSK	Quadrature Phase Shift Keying
RF	Radio-Frequency
RIN	Relative Intensity Noise
RoF	Radio-over-Fiber
TFC	Time Frequency Code
UWB	Ultra-Wide Band
VCSEL	Vertical-Cavity Surface-Emitting Laser

Chapter 1

Introduction

1.1 Background and Motivation

Ultra-Wide Band (UWB) is an emergent technology with deep expected impact on 4th generation wireless communication systems. It can be simply defined as any wireless transmission setup that uses a bandwidth of at least 500 MHz in between the 3.1-10.6 GHz frequency range and a maximum power spectral density of 75 nW/MHz (-41.3 dBm/MHz) [5]. The main advantages of this technology are its reduced complexity and low power consumption, making it suitable for use in commercial wide-band systems, as for example in Wireless Personal Area Networks (WPAN).

UWB signals can be generated using one of three different approaches: short pulses, Orthogonal Frequency Division Multiplexing (OFDM) or Code Division Multiple Access (CDMA) [6]. Either one will generate the large bandwidths necessary for this technology, so the choice of which one to use has to be made according to the desired application requirements, the complexity of the devices and power consumption restrictions. UWB allows for several different data rates, ranging from 53.3 Mb/s to 480 Mb/s. However, a higher data rate usually means a lower range, being just a few meters for its highest rate [4].

With all of these important characteristics, it is clear that UWB is a promising technology for future services where high data rates are needed and short range is not an issue. However, if the advantages provided by UWB signals are desired but longer operating distances are also sought, UWB alone might not be enough - other ways of utilizing these high data rate signals over longer distances need to be investigated. In this way this promising technology can be further applied to a larger variety of applications to suit tomorrow future needs. One such specific case is the recent proposal of UWB technology in the next generation access networks [7].

In this work, we are interested in the investigation of fiber supported UWB signal transmission in order to extend the technology's range - the so-called Radio-over-Fiber (RoF) technology. Specifically, the goal is to design an optical transmitter based on MOS (Metal-Oxide-Semiconductor) technology, capable of operating with UWB signals in the 3.168-3.696 GHz frequency range, by using a vertical-cavity surface-emitting laser (VCSEL). This is carried out by first designing and studying a discrete (PCB-supported) version of the transmitter, followed by its integration using the chosen MOS process. The importance of using a MOS process is due to its ability to deliver very small devices at a cost that might become low enough for them to be used in a widespread manner. The typical setup of optical transmitters in RoF systems using UWB signals can be seen in figure 1.1.

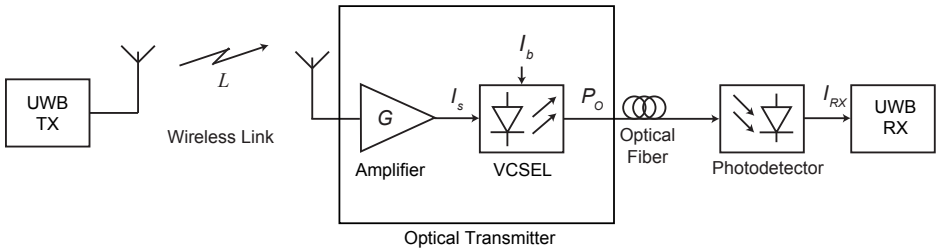

Figure 1.1: Typical setup of an optical transmitter for UWB signals in Radio-over-Fiber systems.

Although a VCSEL integrated circuit driver, specifically for UWB signals in this frequency range, has never been designed to the best of our knowledge, there are nowadays some drivers that are capable of delivering high data throughput (10 Gb/s per VCSEL channel) at a relatively low cost using either a 90 nm [8] or a 130 nm [9] CMOS technology. The former achieves 10 Gb/s by implementing a 4-PAM (Pulse Amplitude Modulation) scheme with equalization in order to compensate for modal dispersion in multi-mode fibers. The latter uses auto-power control and auto-modulation control to obtain constant optical power outputs over a 4-channel VCSEL array, and an active feedback technique for bandwidth improvement. Other examples of VCSEL drivers for multi-Gb/s data rates exist, just like the one detailed in [10].

A complete RoF system for optically transmitting and wirelessly receiving 1.44 Gb/s UWB signals in the 60 GHz band has also been proposed [11] for integrated fiber-to-the-home and WPAN connectivity, employing two different modulation schemes. Specifically, the VCSEL used in the transmitting end (composed of an amplifier, a bias-T and a 1550 nm VCSEL) is directly modulated by the UWB signal, with frequency up-conversion to the 60 GHz being made through a Mach-Zehnder modulator.

These signals are then distributed using optical fiber to the remote sites where they are wirelessly transmitted to a 60 GHz receiver. This receiver will then amplify, filter and down-convert the signal for analysis. Such high data rates were demonstrated for a RoF transmission using a 40 km-long fiber plus 5 m wireless transmission.

1.2 Thesis Organization

After this preliminary introduction chapter, which states the motivations for the development of this project and the main goals to be achieved, the thesis will continue in chapter 2 by presenting the Radio-over-Fiber technology, a mix between optical and wireless networks, since this is the main application for the optical transmitter. In this same chapter, an introduction to VCSEL laser diodes is presented, their properties and theoretical model are given and the basic set of rate equations are explained. Furthermore, an important type of noise generated in laser diodes, the relative intensity noise (RIN), is also discussed since it is also modelled in the system simulations.

In chapter 3 the design steps of the optical transmitter are detailed after a first glimpse on the main RF amplifier design techniques, such as the steps to correctly create the discrete low-noise amplifier (LNA), the VCSEL biasing networks and the matching circuits using transmission lines. Also in this chapter, the techniques for integrating this transmitter using a MOS process are explained, taking into consideration the particularities it presents when compared to the discrete device.

In chapter 4, both versions are actually designed to present the desired performance and their main properties are calculated using the aforementioned techniques.

The thesis proceeds by presenting and explaining, in chapter 5, the simulation results obtained using several different software tools. These results refer to the same properties of both designs of the optical transmitter, allowing one to verify the previously calculated values and to infer on their implications.

In chapter 6 a final conclusion to this thesis is made and future work possibilities are presented.

1.3 Contributions

The work developed in this thesis yielded some contributions related not only to its final results but also to the methods employed to achieve them. Specifically, the contributions are as follows:

- Development of a co-simulation environment to perform simulations using both ADS™ and Matlab™ where the presented EVM simulations have been performed;
- Development of an algorithm to simulate the RIN effects of the VCSEL on the transmitting signal (in collaboration with Nuno Sousa and UTM staff); and,
- Design of a low complexity and low size optical transmitter for UWB signals in the 3.168-3.696 GHz frequency range, both in discrete and integrated circuit versions, presenting an estimated large range, high gain and low overall noise figure.

The work also resulted in one article accepted for presentation at a conference:

- R. S. Maciel, N. Sousa, H. M. Salgado, J.M.B. Oliveira and J. A. M. da Silva, "Optical Transmitter for Ultra-Wide Band signals in the 3.168-3.696 GHz Frequency Range". Conference on Design of Circuits and Integrated Systems (DCIS), November 2012.

Chapter 2

Electro-Optic Converter for RoF Applications

2.1 Introduction

This chapter deals with the optoelectronic components and optical communication systems of concern in this work, namely the VCSEL and RoF systems.

Specifically, the next section details the main characteristics, advantages and disadvantages of systems which integrate in the same network optical and wireless elements - the Radio-over-Fiber technology, which could solve some of the problems currently faced by the users and providers of high data-rate indoor services.

Also, additional details about UWB signals are given, such as their operating frequency, modulation schemes and types of codes used.

The chapter continues by presenting the general structure and main properties of a VCSEL, followed by the small signal frequency response of this type of laser diodes and by the model to be used in the simulations of the transmitter. Here, the rate equations and the VCSEL's equivalent electrical circuit are explained. Also, the origin and main features of the relative intensity noise are given so that it can be also included in the simulations to provide for more reliable results.

The chapter ends with a brief summary of the topics and the main features addressed.

2.2 Optical Systems for RF Signal Transmission (Radio-over-Fiber)

Radio-over-Fiber (RoF) is a technology which involves the integration of wireless and fiber optic networks, usually by using fiber optics to distribute a RF signal from a

central station (CS) to a base station (BS), which is then responsible for emitting the signal to mobile stations (MS). Its main objectives are to increase indoor wireless coverage for a variety of different technologies (UWB, GSM, UMTS, Wireless LAN, etc) and to reuse wavelengths for high data throughput services [12].

With the ongoing increment of services which need large bandwidths and the rising number of their users, the number of BSs will also need to increase in order to meet the demand and, so, it could become imperative that these BSs be simple and low cost. Therefore, in RoF the signal routing and processing functions (such as carrier modulation, frequency conversion, multiplexing) could be only performed at the CS, depending on the architecture used, making it possible for the BS to simply take care of signal amplification, optoelectronic conversion and wireless distribution [1]. A general scheme of a RoF system is depicted in figure 2.1 and it can be noted that the proposed transmitter scheme in figure 1.1 can be viewed as the part of the BS responsible for the wireless signal pre-amplification and electrical-to-optical conversion in the uplink.

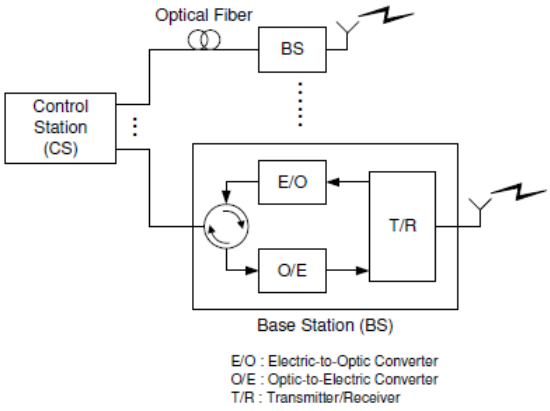

Figure 2.1: General scheme of a RoF system [1].

One of the immediate advantages of this technology is the use of optical fibers to distribute the signals, because they present low attenuation losses at currently used communication wavelengths (0.3 dB/km for 1550 nm and 0.5 dB/km for 1310 nm [13]). Other advantages involve the significantly large bandwidth offered by optical fibers - a very important parameter if the number of BSs increases significantly - as well as their immunity to electromagnetic interference, light weight and smaller sizes when compared to other communication systems, whereas the centralized configuration allows for simpler maintenance and lower costs [1]. However, as this is fundamentally an analogue transmission system, it also presents some disadvantages.

These are related to noise introduction, for example the photodiode noise and the diode laser's Relative Intensity Noise (RIN, see subsection 2.4.4), and distortion of the transmitted signals by the system's components, caused for example by the non-linear distortion of the laser [13].

There are several types of network architectures that can be used in RoF systems and whose main differences are related to the frequency bands used to modulate the optical carriers and distribute the signals from the CS to the BSs. These frequency bands are: base band (BB), intermediate frequency (IF) and radio frequency (RF) [14], making each architecture present its own advantages and disadvantages when employed in RoF systems. For example, BB-over-Fiber architectures present simple optical links and low bandwidth optical components, but they require complex BSs due to the need to locally convert the BB to RF signals. On the other hand, RF-over-Fiber architectures provide the simplest BSs configurations, because the RF signal is provided by the CS which performs frequency up-conversion and other signal processing functions, leaving the BS with only the basic tasks to perform, as previously mentioned. However, this architecture implies the need for high-speed optical components for detecting and generating the RF optical signals, devices that are more expensive and complex. [14].

As mentioned previously, the transmitter/receiver devices at the remote sites can be very simple if the correct architecture is used, comprised of just an antenna, an RF amplifier and a laser/photodetector. In this work, only the transmitter is designed and simulated and, therefore, a laser is used, specifically a VCSEL. A model for this type of laser is detailed later in this chapter.

2.3 UWB Signals

Some of the properties and features of UWB signal technology have already been addressed in the introductory chapter, but these can be further developed in order to present a more complete view of this type of signals. A more detailed description based on the ECMA-368 standard [4] will now be given.

As represented in figure 2.2, the frequency range allocated to the UWB signals used for communications is divided into six different bands, called band groups, using the OFDM multiplexing technique. Each band group is further divided into three sub-bands with 528 MHz of bandwidth each, with the exception being the fifth band group which only has two sub-bands [4]. Despite this wide range of frequencies that can be exploited, the maximum power spectral density is so low (-41.3 dBm/MHz)

that these signals behave like “noise” to other narrowband signals that might exist, avoiding in this way interference effects.

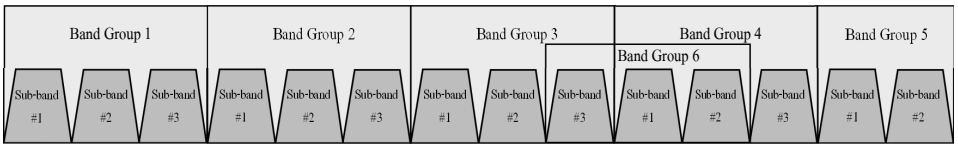

Figure 2.2: Band structure of UWB spectrum.

The 528 MHz bandwidth is divided into 128 subcarriers, thus each one is separated from the neighbours by 4.125 MHz. These 128 subcarriers include data (100), pilot (12), guard (10) or null (6) carriers - for example, the carrier corresponding to the central frequency of a given sub-band is always a null. The data carriers use QPSK (Quadrature Phase-Shift Keying) modulation to achieve data rates up to 200 Mb/s and DCM (Dual-Carrier Modulation) employing a 16-QAM (Quadrature Amplitude Modulation) modulation scheme for data rates from 320 Mb/s up to 480 Mb/s [4]. This is summarized in table 2.1.

Table 2.1: Different modulation schemes and coding rates used for obtaining the several data rates defined for UWB signals [4].

Data Rate (Mb/s)	Modulation	Coding Rate
53.3	QPSK	1/3
80	QPSK	1/2
106.7	QPSK	1/3
160	QPSK	1/2
200	QPSK	5/8
320	DCM	1/2
400	DCM	5/8
480	DCM	3/4

Frequency hopping between sub-bands of the same band group is allowed and 10 different hopping schemes assigned to each band group are defined, called time frequency codes (TFC). These enable the OFDM symbols to be spread (or not) between sub-bands, this way diversifying the frequency slots used and enabling one to distinguish between different users [2]. Time-domain spreading and forward error correction (FEC) coding with different coding rates can also be used to help change the data rates for the cases when the same modulation is employed. This is also indicated in table 2.1, where a coding rate of x/y means that only x bits out of y bits are coded.

2.4 VCSEL

2.4.1 Structure and Properties

VCSELs are a type of semiconductor laser diode in which the emitted light comes out perpendicular to its surface. The laser's cavity is made using two Bragg mirrors and the active medium is usually comprised of several quantum wells (figure 2.3), with a total thickness of just a few micrometers. This active region is electrically pumped by a ring electrode with typically a few tens of mW of power, generating an output power from the laser up to 5 mW for single mode devices [15]. However, several other configurations for current injection and confinement within the active region are possible, each one presenting its own advantages and disadvantages to commercial use [16].

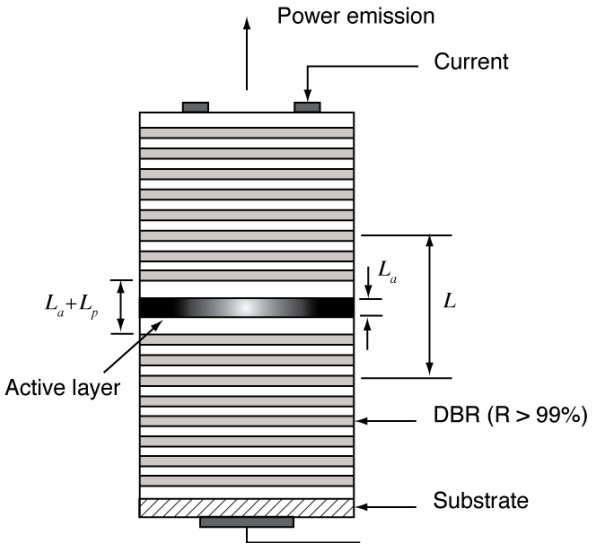

Figure 2.3: General VCSEL structure, indicating the active region's length (L_a) [2].

Giving the fact that this is a very small device it becomes fairly easy to obtain single frequency operation of the laser. However, due to these small dimensions and due to the fact that it is harder to uniformly pump a larger active region, more transverse modes can be excited if higher mode areas and, thus, higher output powers are desired, hence deteriorating the beam's quality [15]. Also, VCSELs have low beam divergence when compared to edge-emitting lasers and a symmetric beam profile, making it easy to collimate their output. Other important advantages of VCSELs include the very low threshold levels (µA level), the insensitivity of wavelengths to temperature variation, high-speed modulation capabilities (more than 10 Gb/s in some cases), long lifetimes (up to 10^7 hours in room-temperature operation) and

lower overall costs, arising from its vertical-cavity structure which gives the ability for testing each laser at intermediate stages of production and not just at the end [16].

Several wavelengths can be obtained using these devices, depending on the type of semiconductor material that makes the active region and its surroundings. These wavelengths span a broad spectrum, from the long-wavelength band (1.3/1.55 µm), passing through the mid-wavelength band (0.98 µm) and the near-infrared band (0.78/0.85 µm) up to the green-blue UV band. For example: 1.3 µm or 1.55 µm wavelengths can be obtained with a GaInAsP-InP system with various types of mirror materials; 0.98 µm wavelengths can be obtained with a GaInAs-GaAs system providing threshold currents as low as a few hundreds of µA; and, GaAlAs-GaAs systems can be used for 0.85 µm wavelength emission [16].

2.4.2 Model

In order for the simulations of the transmitting system to be made a model of the VCSEL must be used so that its behavior can be correctly analyzed and predicted. This model is presented here, consisting of the rate equations and of the VCSEL's equivalent electrical circuit, which includes the parasitic components caused by the laser package and chip. This equivalent circuit is of extreme importance when dealing with high frequencies because the frequency limits of the system will usually be defined by its parasitic components, therefore contributing to the response of the laser to the input signal.

The rate equations for a VCSEL, which account for all processes that occur inside the semiconductor material and that will affect the carrier (N) and photon density (P), can be expressed as [2]

$$\frac{dN}{dt} = \frac{\eta_i I}{qV} - \frac{N}{\tau} - R_{st}P \tag{2.1}$$

$$\frac{dP}{dt} = \Gamma R_{st}P - \frac{P}{\tau_p} + N\beta\Gamma R_{sp} \tag{2.2}$$

where η_i is the injection efficiency, V is the volume of the active region, I is the electrical current, q is the value of the electron charge, τ is the carrier lifetime, Γ is a confinement factor, R_{st} and R_{sp} are the stimulated and spontaneous emission rates, respectively, τ_p is the photon lifetime inside the cavity and β is the fraction of the total spontaneous emission coupled into the laser mode.

Equation 2.1 describes the rate of change of the carriers' density N in the semiconductor. The first term accounts for the rate at which electrons or holes are injected into the active layer due to external pumping; the second term introduces the losses of the carriers through spontaneous emission and non-radiative recombination; and the last term accounts for those carriers that recombine through stimulated emission and, therefore, contribute to the lasing process. In this last case the term can be approximately written as [2]

$$R_{st}P = v_g g(N)P \approx v_g a(N - N_{0m})(1 - \epsilon P)P \tag{2.3}$$

where v_g is the laser's group velocity, $g(N)$ is the stimulated gain function, $a = \frac{\partial g}{\partial N}$ is the differential gain, N_{0m} is the carrier density at zero gain and $(1 - \epsilon P)$ is a phenomenological term describing gain compression, with ϵ being the gain compression factor with units of m^3. The approximation for the stimulated gain function has been made by simply writing the initial logarithmic expression for $g(N)$ in a Taylor series.

In equation 2.2, which describes the rate of change of the photons' density inside the cavity, the first term is due to the coherent photon generation through stimulated emission, the second term accounts for the loss of photons from the cavity - with the photon lifetime inside the cavity being given by $\frac{1}{\tau_p} = v_g \left[\alpha_s + \frac{1}{L} ln \left(\frac{1}{R}\right)\right]$, and the last term accounts for the rate of spontaneously generated photons. In this equation the first term can also be approximated by eq. 2.3, just like in the case of eq. 2.1 [2].

By measuring the frequency response of the laser at several bias currents, the frequency subtraction method permits the extraction of the laser parameters, making it possible to accurately simulate the behavior of a real device [17]. In this way, the standard values that will be used were taken from [17, 18] and are given in table 2.2.

Table 2.2: Laser parameters used.

Parameter	Value	Unit
V	2.4×10^{-18}	m^3
g_0	4.2×10^{-12}	$\mathrm{m}^3\mathrm{s}^{-1}$
ϵ	2.0×10^{-23}	m^3
N_{0m}	1.9×10^{24}	m^{-3}
β	1.7×10^{-4}	-
Γ	4.5×10^{-2}	-
τ_P	1.8	ps
τ_S	2.6	ns
η_i	0.8	-
I_{th}	0.893	mA

As far as the VCSEL's equivalent electrical circuit is concerned, figure 2.4 represents the model used - a RLC resonant [2] circuit acting as a low-pass filter with a cutoff frequency of 7.4 GHz (measured with ADS™). It is comprised of an inductor L_P, a capacitor C_P and a resistor R_S (the so-called parasitic components) in series with the active region (intrinsic laser diode (ILD)) described by the aforementioned rate equations. Above threshold this ILD can be electrically viewed as a short-circuit at all frequencies when comparing to other relatively large components' impedances which make up the circuit model [2]. These values of the components were taken from [19] and are given in table 2.3.

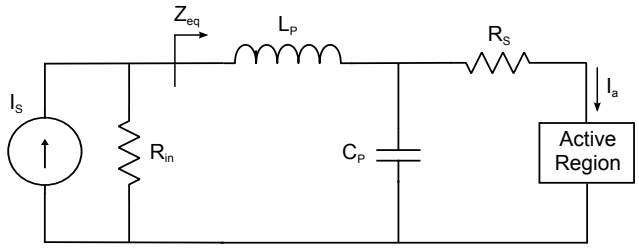

Figure 2.4: VCSEL equivalent circuit of the laser parasitics.

Table 2.3: Values of the parasitic components.

Component	Value	Unit
R_S	76	Ω
C_P	0.39	pF
L_P	2.28	nH

The components L_P and C_P are due to the laser package and represent the wire-bond inductance and the contacts capacitance, respectively. The series resistor R_S represents the contacts resistance as well as the Bragg mirror stacks [2] (Distributed Bragg Reflectors (DBR) elements in figure 2.3).

The frequency behavior of this equivalent circuit model (assuming that the ILD is a short-circuit, as already explained) can be described by means of its equivalent impedance Z_{eq}, given by

$$Z_{eq} = \frac{R_S}{1 + R_S^2 C_P^2 \omega^2} + j\left(\omega L_P - \frac{\omega R_S^2 C_P}{1 + R_S^2 C_P^2 \omega^2}\right) \tag{2.4}$$

2.4.3 Small Signal VCSEL Response

The VCSEL rate equations can be linearized if one considers the small signal response of the laser. In these conditions, the transfer function of the laser can be found for

different bias currents. An example is given in figure 2.5, where the magnitude of the first-order transfer function $H(f)$ (defined as the ratio of the photon density to a perturbed current) is presented for 3 mA and 6 mA bias currents. This transfer function represents the frequency response of both the laser and its equivalent electrical circuit discussed in the previous subsection.

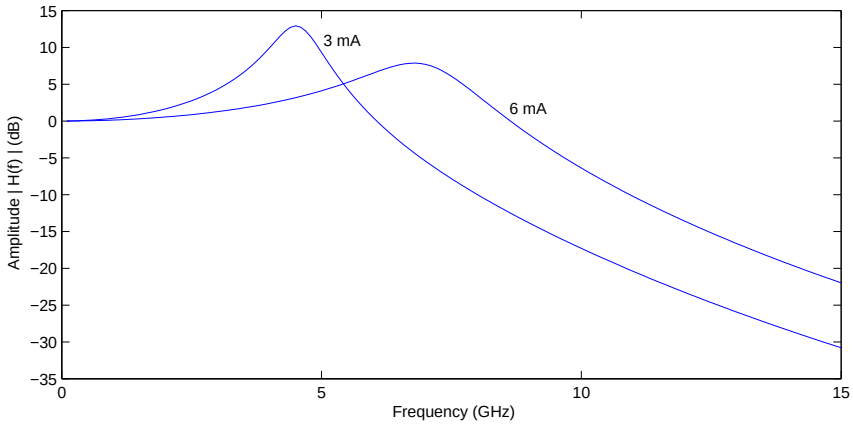

Figure 2.5: Small signal transfer function of the VCSEL.

It can be seen that for the highest bias current the peak has a lower value and is at a higher frequency than the 3 mA peak, this way increasing the available modulation bandwidth and flattening the overall behavior. Without considering other effects in the laser, this is expected to continue to happen with increasing currents until the limit is reached [20].

2.4.4 Relative Intensity Noise

In all kinds of lasers, and VCSELs in particular, noise is an intrinsic random process which plays an important role in defining the quality of the output laser beam. This beam, in the case of lasers which are used in optical communication systems, is responsible for the transmission of data. Therefore, its quality is of extreme importance because it will be related to the definition of several important properties of the system, such as its maximum range and bit error rate (BER). In VCSELs and other types of semiconductor laser diodes, the noise can be generated by spontaneous emission of photons or by carrier generation or recombination processes.

It is clear that an understanding of the noise generated in these kind of devices is important to correctly model their behavior and to adequately simulate the transmitting system. Although a complete description of noise in semiconductor laser diodes

relies on a quantum formulation of the rate equations, a semiclassical approach usually suffices in describing its behavior.

In this way, the time-dependent optical power emitted from a VCSEL can be described in the following way

$$P(t) = \langle P(t) \rangle + \delta P(t) \tag{2.5}$$

where $\langle P(t) \rangle = P_0$ is the steady-state photon density and $\delta P(t)$ represents the noise added to the signal. The intensity noise at a given frequency can be characterized by the relative intensity noise (RIN) [2]

$$RIN = \frac{S_p(\omega)}{P_0^2} \tag{2.6}$$

where $S_p(\omega)$ is the power spectral density of the random process $\delta P(t)$ given by the Wiener–Khinchine theorem

$$S_p(\omega) = \int_{-\infty}^{\infty} \langle \delta P(t+\tau) \delta P(t) \rangle \, e^{-i\omega\tau} d\tau \tag{2.7}$$

Usually the RIN is defined in dB/Hz. Re-writing eq. 2.6 to explicitly show the dependence on the signal bandwidth Δf and to obtain the value in dB, we get [21]

$$RIN = 10 \log_{10} \left(\frac{\langle \delta P(t)^2 \rangle}{P_0^2 \Delta f} \right) \tag{2.8}$$

where $\langle \delta P(t)^2 \rangle$ represents an averaged value of the square of the noise total power. From here, and considering a photodetector with a given responsivity $r = \frac{I}{P}$, it is fairly straightforward to obtain the noise current as a function of the signal's optical power

$$\left\langle I^2 \right\rangle_{RIN} = P_0^2 r^2 10^{\frac{RIN}{10}} \Delta f \tag{2.9}$$

The RIN spectrum does not present a constant behavior because it has a specific peak at a given resonance frequency for a single mode device and several peaks for multi-mode ones [21]. However, below and above these frequencies the RIN spectrum is considerably flat and in the simulations it will be assumed that the VCSEL is operating in these regions.

2.5 Summary

This chapter presented the main features of a technology which merges optical and wireless networks, the Radio-over-Fiber technology. This technology allows for better

coverage for services which need high data-rates by using the best properties of both worlds, like the low losses and high bandwidths of fiber optics and the mobility of RF wireless links. It is a technology which can present lower costs and can be used indoors as well as outdoors, by replacing other wired systems. It is clear that it presents several advantages over other competing communication systems (which use coaxial lines or are based only on wireless networks) for some applications and its use is, therefore, expected to increase in the next years.

More details of UWB signals have also been given, namely the fact that they use either QPSK or DCM modulations depending on the data rates desired and that these signals are generated using OFDM techniques. Some of the codes these signals use for varying the data rates and distinguishing between users, like TFC and FEC codes, respectively, have also been presented.

The other topic focused during this chapter was the VCSEL. It was explained that it can be made of several cascaded quantum wells and that its particular structure provides properties to the laser beam which can be very appreciated in some applications, such as an easier to obtain monochromaticity, good beam symmetry and lower costs when compared to edge-emitting diode lasers. Moreover, the VCSEL's rate equations were detailed and its equivalent electrical circuit model was presented, noting that it acts as a low-pass filter with cutoff frequency of 7.4 GHz. These allow one to be able to reliably predict the VCSEL's dynamic behavior in the simulations. Another aspect covered concerns a very important type of noise occurring in diode lasers - the RIN. This noise is always present, having a peaked spectrum with flat behavior far from the resonance frequencies. A description of the RIN is needed in order to make the simulations even more reliable.

Chapter 3

Design of RF Amplifiers

3.1 Introduction

This chapter deals with the main techniques used to design the LNA needed for the transmitter, whether that be with discrete commercial off-the-shelf (COTS) components or by using a MOS process. Each technology to be used presents features that make these techniques different, so they must be detailed separately.

The following section will introduce some of the techniques that have been used to design the discrete version of the LNA. These will allow one to obtain the desired features when designing the actual device later on and to assess its properties like, for example, the stability conditions, the gain and the whole ensemble noise.

The techniques for designing an analogue microelectronics amplifier for integrating the transmitter using a MOS process are detailed afterwards. In this section, the main concerns and differences from the design of the discrete version are also explained, justifying the need to consider some new effects while neglecting others.

This chapter is finalized with a brief summary of the main conclusions.

3.2 Techniques for Designing Discrete RF Amplifiers

One of the most important components of our transmitter is the LNA, which will be used to amplify an input signal before it can be fed into the VCSEL and transmitted over an optical fiber. The PCB version of this amplifier should then be designed carefully, using transmission line theory due to the high operating frequencies and relatively large dimensions, as any problem it possesses can significantly affect the information to be transmitted.

In order for an amplifier to behave properly and not oscillate when an input signal is applied, its frequency stability should be verified. This verification can be made using the $K - \Delta$ test based on the transistor's scattering-parameters (S-parameters) [22]:

$$K = \frac{1 - |S_{11}|^2 - |S_{22}|^2 + |\Delta|^2}{2\,|S_{21}S_{12}|} > 1 \tag{3.1}$$

$$|\Delta| = |S_{11}S_{22} - S_{21}S_{12}| < 1 \tag{3.2}$$

where K is called the stability factor.

The S-parameters are specific to an electrical system or network and they relate the reflected voltages with the incident ones. For example, for a two-port network (figure 3.1), the S-parameters' matrix is defined as [22]:

$$\begin{pmatrix} V_1^- \\ V_2^- \end{pmatrix} = \begin{pmatrix} S_{11} & S_{12} \\ S_{21} & S_{22} \end{pmatrix} \begin{pmatrix} V_1^+ \\ V_2^+ \end{pmatrix} \tag{3.3}$$

where V_1^-/V_2^- are the reflected voltages at port 1/port 2 and V_1^+/V_2^+ are the incident voltages.

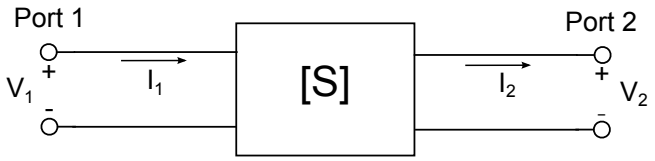

Figure 3.1: Schematic diagram of a 2-port network.

If the $K - \Delta$ test conditions are not satisfied that means the amplifier is conditionally stable (or potentially unstable). In this case, the stability circles for the source and the load must be obtained in order to find the appropriate matching conditions between the source and the load and the amplifier itself, in order to guarantee a stable behavior.

After the stability of an amplifier is assessed, one should start thinking on how to obtain the desired gain. Figure 3.2 represents a diagram of an amplifier, which includes a transistor, supposed to be described by the S-parameters, and the corresponding matching circuits at the input and output. The overall transducer gain of an amplifier is basically dependent on its intrinsic power gain (G_0, given by the transistor's $|S_{21}|^2$) and on the impedance matching sections used, as can be seen from the next relation [22]

$$G_T = G_S G_0 G_L = \frac{1 - |\Gamma_S|^2}{|1 - \Gamma_{in}\Gamma_S|^2} |S_{21}|^2 \frac{1 - |\Gamma_L|^2}{|1 - S_{22}\Gamma_L|^2} \tag{3.4}$$

where the first factor corresponds to the gain associated with the matching circuit of the source impedance and the last one to the gain associated with the matching circuit of the load impedance. $\Gamma_{S/L}$ is the source/load reflection coefficient and Γ_{in} is the transistor's input reflection coefficient. The input and output reflection coefficients for a 2-port system are defined as

$$\Gamma_{in} = S_{11} + \frac{S_{12}S_{21}\Gamma_L}{1 - S_{22}\Gamma_L} \tag{3.5}$$

$$\Gamma_{out} = S_{22} + \frac{S_{12}S_{21}\Gamma_S}{1 - S_{11}\Gamma_S} \tag{3.6}$$

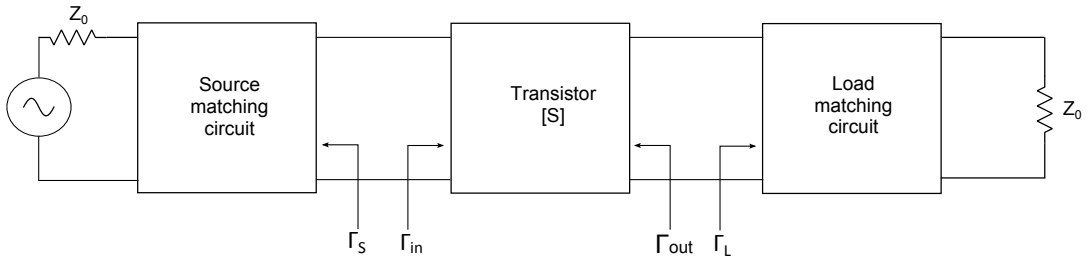

Figure 3.2: Diagram of a typical amplifier, including a transistor and its corresponding source and load matching circuits.

As an example, if one wants the maximum transducer gain for a given amplifier the source and load impedances need to be perfectly matched to the amplifier input and output impedances, respectively; that is, $\Gamma_S = \Gamma_{in}^*$ and $\Gamma_L = \Gamma_{out}^*$. This is called conjugate matching and in this case the transducer gain is simply given by

$$G_T = \frac{1}{1 - |\Gamma_S|^2} |S_{21}|^2 \frac{1 - |\Gamma_L|^2}{|1 - S_{22}\Gamma_L|^2} \tag{3.7}$$

If the amplifier is unilateral, that is, $S_{12} = 0$, then eqs. 3.5 and 3.6 simplify to

$$\Gamma_{in} = S_{11}$$

$$\Gamma_{out} = S_{22}$$

and the gain calculation becomes even simpler

$$G_{TU} = \frac{1}{1 - |S_{11}|^2} |S_{21}|^2 \frac{1}{1 - |S_{22}|^2} \tag{3.8}$$

It should be noted that this gain is not exactly correct if a S_{12} parameter exists, which in reality it does even if it is quite small. But in these cases the difference between the unilateral gain and the real gain is also small, so if the S_{12} parameter is indeed insignificant the unilateral gain equation is used in order to simplify calculations and to provide a gain estimate for future circuit optimization. By using the unilateral figure of merit, U, defined as

$$U = \frac{|S_{11}|\,|S_{22}|\,|S_{21}|\,|S_{12}|}{\left(1 - |S_{11}|^2\right)\left(1 - |S_{22}|^2\right)} \tag{3.9}$$

the error made by this simplification can be bounded in the following way

$$\frac{1}{(1+U)^2} < \frac{G_T}{G_{TU}} < \frac{1}{(1-U)^2} \tag{3.10}$$

Usually, a maximum value of $U = 0.1$ is desired for the unilateral approach to be considered acceptable, because it brings an error of less than $\pm 1\, dB$ [23].

Impedance matching can be achieved in several ways, but since this is a RF circuit one should not use lumped elements but transmission lines instead, as already discussed. One of the main techniques for impedance matching uses stubs, that is, transmission lines in short or open-circuit placed at a specific distance from the unmatched impedance using a connecting line, as represented in figure 3.3. In this way, the input impedance of the circuit is controlled by the parameters of the transmission lines. It should be noted that for microstrip lines (figure 3.4), which are the type of lines that will be used, open-circuits are usually preferred due to simplicity of fabrication. It should also be noted that an unconditionally stable amplifier can always be designed for maximum gain, since it can present any desired reflection coefficient for a stable behavior.

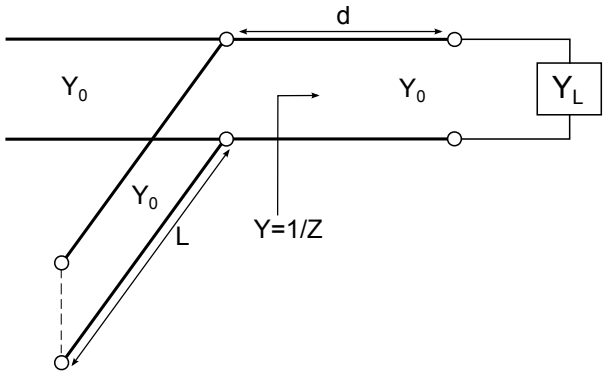

Figure 3.3: Matching circuit using stubs: L is the length of the stub and d is its length position along the transmission line.

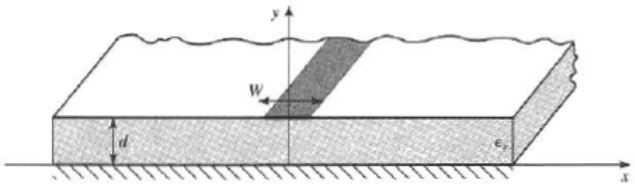

Figure 3.4: Microstrip line model: d is the thickness of the substrate with ϵ_r permittivity and W is the width of the line [3].

However, if a specific gain is given that does not correspond to the maximum possible one, then an impedance mismatch needs to be intentionally created so that the amplifier's total gain matches the one desired. The amount of mismatch can be found from eq. 3.4, by simply obtaining the reflection coefficients Γ_S and Γ_L. Then, it is just a matter of obtaining the necessary stub parameters with a Smith Chart to get an amplifier with the desired gain [22].

As far as the noise figure of the amplifier is concerned - a parameter of great importance in low noise systems - it can be computed using the Friis formula, an expression suitable for receiving systems comprised of cascaded components which present gain and noise generation and usually defined as [3]

$$F_T = F_1 + \frac{F_2 - 1}{G_1} + \frac{F_3 - 1}{G_1 G_2} + ... \tag{3.11}$$

where F_1 represents the noise figure of the receiver's first component and G_1 its gain, and so on to as many components as the cascaded system presents.

For the specific case of a single transistor, its noise figure can be determined using [22]

$$F = F_{min} + \frac{4R_{\frac{N}{50}} \left|\Gamma_S - \Gamma_{opt}\right|^2}{\left(1 - \left|\Gamma_S\right|^2\right) \left|1 + \Gamma_{opt}\right|^2} \tag{3.12}$$

where $R_{\frac{N}{50}}$ is the transistor's equivalent noise resistance referenced to 50 Ω, Γ_{opt} is the source reflection coefficient which determines the minimum noise and F_{min} is the minimum noise figure (when $\Gamma_S = \Gamma_{opt}$).

3.3 Integration Using a MOS Process

To design the integrated version of our transmitter one must account for some issues that were not addressed during the design of the discrete version and that are now of extreme importance. Such issues are related to the size and non-idealities of the components placed in the circuit and their layout, which will certainly influence the IC's performance. Common non-idealities include intrinsic parasitic effects in the components (like the transistors, bondpads and bonding wires) which arise from their physical implementation and which can be minimized through, for example, size reduction. Thus, the correct design and layout of the components that make this transmitter will allow one to reduce the total intrinsic effects. Nevertheless, they will always exist and, therefore, need to be considered in the simulations.

Since the layout of the integrated circuit is one of the main goals of this work, it should be noted that its creation is governed by some rules to ensure its appropriate operation when considering the presence of the aforementioned component - and even production materials - non-idealities. These rules are related not only to the transistor layout, but also to all other elements which make the integrable circuit.

3.3.1 Analogue Microelectronics Theory

Some of the theory for assessing a RF circuit's properties has already been addressed in section 3.2, as they are essentially the same whether we are considering a PCB or an IC.

However, the design of an analogue microelectronics circuit is very different from the design of a circuit based on discrete components. In this case, since one needs to design the transistors themselves, their models need to be studied and their dimensions need to be correctly found because the system's properties may vary considerably with them - for example, a bigger transistor can provide higher gain but it will also have larger intrinsic components (mainly capacitances between its terminals) which will worsen the behavior at higher frequencies.

In this way, the small-signal equivalent circuit model of a field-effect transistor (FET) is represented in figure 3.5, showing a grounded source terminal and including

the effect of channel-length modulation through the resistance r_o [24], as well as some intrinsic elements (such as the capacitances C_{GS} and C_{GD}).

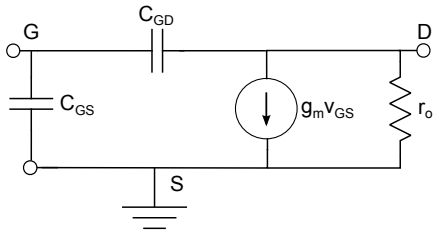

Figure 3.5: Small-signal equivalent circuit model of a FET when considering the channel-length modulation effect and some intrinsic capacitances.

The transistor's physical dimensions when neglecting channel-length modulation can be found using the following expression[25]

$$\frac{W}{L} = \frac{g_m}{\mu C_{ox} V_{GSef}} \tag{3.13}$$

where W is the transistor's width and L its length, $g_m = \frac{2I_{DS}}{V_{GSef}}$ is the transconductance, μC_{ox} is the transistor's intrinsic transconductance and $V_{GSef} = (V_{GS} - V_T)$ is the effective gate-to-source voltage.

It is the transconductance of a transistor together with its output resistance (R_{out}, which is dependent on the load of the transistor) which determines the gain, as given by the following expression

$$A = g_m R_{out} \tag{3.14}$$

However, the achievement of this gain is dependent not only on the transistor itself but also on external factors, such as impedance matching. Impedance matching can be achieved in more than one way, but in this case it will be used the scheme of figure 3.6 for input matching. It should be noted that since IC connections inherently present lower physical dimensions than a common PCB's, their design is made without considering transmission lines nor their consequent circuit design implications, such as in impedance matching - hence the lumped elements used in the matching scheme. This is because the lowest operating signal wavelength is approximately 8 cm, a very large value compared to typical IC lines' dimensions.

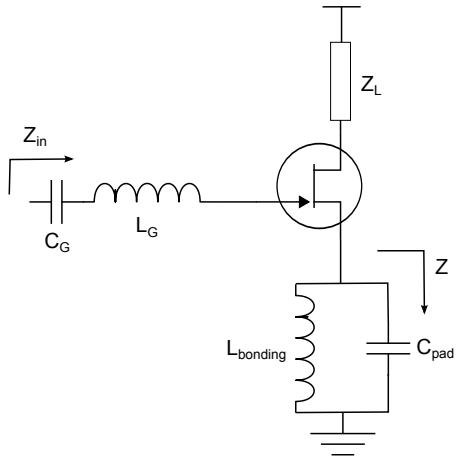

Figure 3.6: Input impedance matching scheme used.

In figure 3.6, an inductance (L_G) is used in series with the capacitance used for DC-coupling (C_G) to match the input impedance of the transistor to the source's impedance. This input impedance is given by [25]

$$Z_{in} = -j\frac{1}{\omega C_{GS}} + Z + \frac{g_m Z}{j\omega C_{GS}} \tag{3.15}$$

where Z is the bondpad and bonding wire equivalent impedance (refer to figure 3.7 for their equivalent model), which usually becomes $Z \approx j\omega L_{bonding}$ for small values of bondpad capacitance (C_{pad}). This model for the transistor's input impedance does not take into account the gate resistance, the gate-to-drain capacitance (C_{GD}, whose input effect can become very large due to the Miller effect), the output resistance or other intrinsic components and, therefore, it will be used just as a guiding model for later tuning.

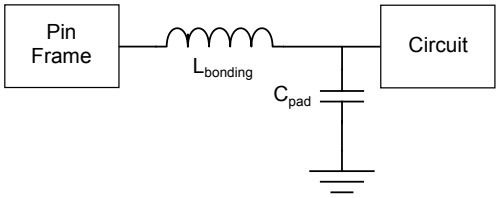

Figure 3.7: Bondpad and bonding wire model.

As can be seen this input impedance is mainly capacitive, but it also presents a real part. If one wants to match this impedance to a 50 Ω source the imaginary part would need to be zero and the real part 50 Ω, yielding the following conditions for

the components [25]

$$f_0 = \frac{1}{2\pi\sqrt{(L_{bonding} + L_G)\left(\frac{C_{GS}C_G}{C_{GS}+C_G}\right)}} \tag{3.16}$$

$$\frac{g_m L_{bonding}}{C_{GS}} = 50 \tag{3.17}$$

The output matching can be considerably simpler since the channel resistance r_o is considered infinite (no channel-length modulation effect), making the output impedance only dependent on the bondpad and bonding wire equivalent impedance (typically very small), on the C_{GD} capacitance referred to the output (Miller effect) and on the output DC-coupled capacitor (C_{out}). Hence, the output impedance is found to be solely capacitive, but in reality this is not completely true because a real part is always present. Nevertheless, the DC-coupled capacitor C_{out} can be used to obtain good matching because its value can be (almost) freely changed.

3.4 Summary

In this chapter, some of the techniques that are needed to assess the properties of the discrete LNA and to obtain the desired features in the implementation stage were presented, including how impedance matching should be made to obtain the needed reflection coefficients.

Then, the basic theory for designing analogue microelectronic circuits was presented, in order to enable the integration of the transmitter using a MOS process. In this section, several design constraints that appear only when using these technologies were explained so that they can be considered in the circuit design and simulation. For example, the fact that IC design implies small connection dimensions means that impedance matching is not necessary between components inside the chip and that lumped elements can be used for input and output impedance matching.

Chapter 4

Design of the Optical Transmitter for a 3.168-3.696 GHz UWB Signal

4.1 Introduction

This chapter deals with the design of the optical transmitter for UWB signals in the 3.168-3.696 GHz frequency range, which is basically comprised of a RF low-noise amplifier (LNA) plus the VCSEL and its biasing circuit. Specifically, one wants to design a LNA for the 4 GHz limit to allow for the amplification of the signals in the desired frequency band, before they can be fed into the VCSEL for electrical-to-optical conversion and consequent fiber transmission. This LNA, in its discrete version, is comprised of two cascaded single-voltage enhanced-mode pHEMT (pseudomorphic High Electron Mobility Transistor) transistors from Avago Technologies, designed for maximum gain. In the integrated version, the LNA will also be made of two transistors designed using a specific process. To complete the description of the transmitter, the next section will present its general structure.

Then, the techniques presented in the previous chapter are applied to specifically calculate the main properties of the discrete LNA, like its frequency stability, maximum unilateral gain and noise figure.

After that, the biasing networks used to correctly bias both transistors and the VCSEL are presented, indicating the components used and showing how they were obtained to provide for proper transistor or VCSEL operation, without ignoring their effects on the whole transmitter.

Then, the steps taken towards obtaining the desired source and load reflection coefficients for getting the maximum gain are presented by explaining the impedance matching circuits designed for the discrete LNA.

The following section presents the MOS process used in the integration of the transmitter, as well as its main features.

The integration of this device using a MOS process with the microelectronics theory previously presented is detailed afterwards, providing some of the specific characteristics of this circuit and its components, like the transistor's dimensions and gain.

This chapter is finalized with a brief summary of the main results and conclusions presented herein.

4.2 General Structure of the Transmitter

The transmitter to be designed presents a simple structure: three matching networks which allow for impedance matching between components of the device, two transistors which provide amplification and their biasing circuit, a VCSEL for electrical-to-optical conversion and also its biasing circuit. A block diagram representing this structure is depicted in figure 4.1, which is the same no matter which design version is being considered.

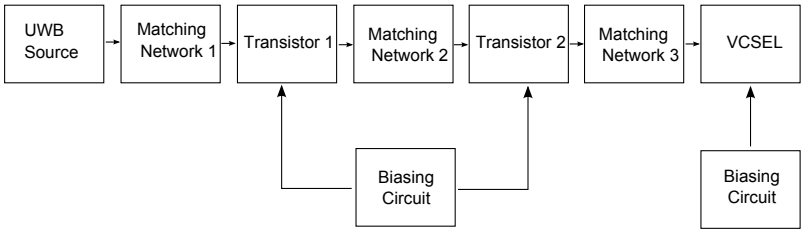

Figure 4.1: General scheme of the transmitter to be designed.

A detailed explanation of the design of the electrical components which make this device is given in the following sections.

4.3 Properties of the Amplifier

4.3.1 Frequency Stability

By utilizing the $K - \Delta$ test discussed in section 3.2, this key parameter for every amplifier has been assessed, with eqs. 3.1 and 3.2 yielding the following results

$$K = 0.896 < 1$$

$$|\Delta| = 0.268 < 1$$

for the following transistor S-parameters (at 4 GHz) [26]

$$S_{11} = 0.513\angle 175.4^{\circ}$$

$$S_{21} = 5.13\angle 49.1^{\circ}$$

$$S_{12} = 0.075\angle 14.2^{\circ}$$

$$S_{22} = 0.345\angle -74.3^{\circ}$$

These results show that the LNA is conditionally stable at the chosen design frequency (4 GHz). As previously stated, the stability circles need to be found in order to design the amplifier's matching circuits using stable reflection coefficients. The source and load stability circles for each transistor obtained with ADS™ are pictured in figure 4.2, as well as the reflection coefficients $\Gamma_S = S_{11}^*$ and $\Gamma_L = S_{22}^*$ represented by the red dots in each circle, which provide maximum unilateral gain. Moreover, since $|S_{11}| < 1$, the center of the Smith chart ($\Gamma_{S/L} = 0$) belongs to a stable region.

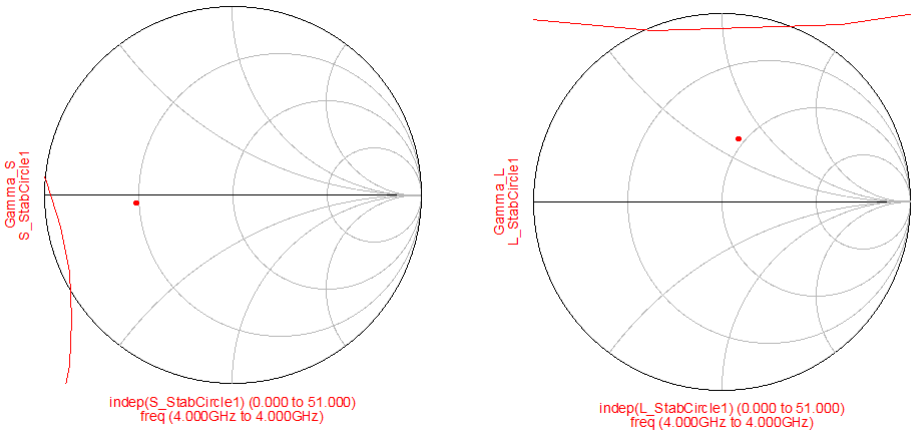

(a) Source stability circle and Γ_S. (b) Load stability circle and Γ_L.

Figure 4.2: Stability circles for the amplifier at 4 GHz with the used reflection coefficients.

It can be clearly seen from the figure that for these values of $\Gamma_S = S_{11}^*$ and $\Gamma_L = S_{22}^*$ the amplifier is stable and with enough distance from the unstable region to allow for some stability margin. Hence, despite this amplifier being potentially unstable at 4 GHz, it was still possible to design it with a gain equal to the maximum unilateral gain. Furthermore, it has been confirmed that, despite this amplifier being also potentially unstable throughout the entire signal frequency band, the choice of $\Gamma_S = S_{11}^*$ and $\Gamma_L = S_{22}^*$ still provides a stable behavior at all these frequencies.

4.3.2 Gain

The gain of the LNA is given by the gain of each of its composing transistor's and depends on the matching obtained with the impedance matching networks, as already explained in section 3.2. With the reflection coefficient values given in the previous subsection we can easily calculate the unilateral gain of each transistor and of the whole amplifier.

In this way, by using eq. 3.7 and the corresponding reflection coefficients, the maximum gain for each transistor is

$$G_{Max} = 1.34\,dB + 14.2\,dB + 1.14\,dB = 16.1\,dB$$

and, hence, the ensemble's total gain is simply

$$G_{LNA} = 2 \times G_{Max} = 32.2\,dB$$

Since this is the unilateral gain the error to the actual gain can be estimated. The unilateral figure of merit for each transistor is obtained using eq. 3.9 and the component's S-parameters, giving

$$U = 0.10$$

which is the maximum allowed value for considering a unilateral approach. From eq. 3.10, where $G_{Max} = G_{TU}$, this bounds the error in the following way

$$0.83 < \frac{G_T}{G_{TU}} < 1.23$$

and, in dB,

$$-0.81\,dB < G_T - G_{TU} < 0.89\,dB$$

From these values we can conclude that the unilateral assumption gives a transducer gain with an error within 1.7 dB. However, should the U parameter be a little

higher, the amplifier would need to be designed considering the more realistic bilateral behavior so that a higher error could be avoided.

4.3.3 Noise Figure

By replacing the constants in eq. 3.12 with the ones specific of the chosen transistors [26] (available only at a frequency of 3.9 GHz) and by using $\Gamma_S = S_{11}^*$ as previously discussed, the noise figure for each transistor is obtained, giving

$$F = 0.98\, dB$$

With these noise figures and with the gain value determined in the previous section, we can compute the LNA's noise figure by making $F_1 = F_2 = 1.25$ (0.98 dB) and $G_1 = 40.7$ (16.1 dB) in eq. 3.11, giving

$$F_{LNA} = 1\, dB$$

It is expected that the noise figure be lower at the operating frequencies, since this value was obtained for a higher frequency.

4.4 Transistors' Biasing Network Design

The two transistors used in this transmitter need to be correctly biased in order to ensure its appropriate operation. In this case a single circuit will be used to bias both transistors to simplify the final overall circuit.

The circuit used for this purpose is represented in figure 4.3. This circuit is based on the one provided in the transistor's datasheet [26] and it is a passive type of biasing network comprised of a 5 V source, several resistors, capacitors and high impedance $\lambda/4$ transmission lines (components T_1 and T_2 in the figure). The resistors contribute to current limitation, voltage division and improved low frequency stability; the C_1 and C_4 capacitors provide the DC-coupling; and the other capacitors and the $\lambda/4$ transmission lines provide the required isolation between the signal and biasing networks. The high impedance $\lambda/4$ transmission lines are used instead of inductors to provide for better performance at high operating frequencies.

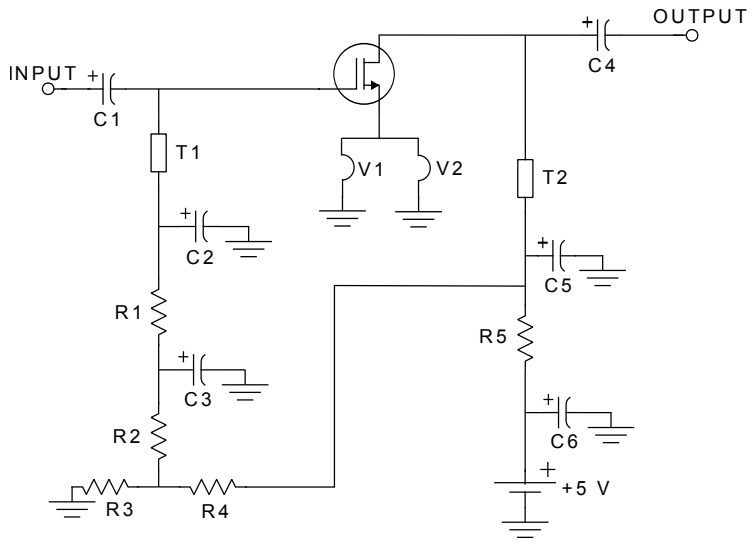

Figure 4.3: Scheme of the biasing network used to bias both transistors (T_1 and T_2 are the $\lambda/4$ transmission lines).

The bias conditions for each transistor which correspond to our S-parameters are [26]

$$V_{DS} = 3V$$

$$I_{DS} = 20\,mA$$

To obtain similar conditions, the values chosen for the components of figure 4.3 are indicated in table 4.1.

Table 4.1: Values of the components used in the biasing network.

Component	Value	Unit
C_1	10	pF
C_2	10	pF
C_3	0.1	μF
C_4	10	pF
C_5	10	pF
C_6	0.1	μF
R_1	10	kΩ
R_2	10	kΩ
R_3	940	Ω
R_4	5060	Ω
R_5	50	Ω
T_1, T_2(length)	549.3	mil
T_1, T_2(width)	9.9	mil

Some of these values are given in [26], like for the components C_3, C_6, R_1 and R_2, but others were calculated using simple DC circuit analysis. Such is the case of resistors R_3, R_4 and R_5, whose values were obtained using [26]

$$R_3 = \frac{V_{GS}}{I_{BB}} \tag{4.1}$$

$$R_4 = \frac{(V_{DS} - V_{GS})\, R_3}{V_{GS}} \tag{4.2}$$

$$R_5 = \frac{V_{DC} - V_{DS}}{I_{DS} + I_{BB}} \tag{4.3}$$

where $V_{GS} = 0.47\,V$, $I_{BB} = 0.5\,mA$ and $V_{DC} = 5\,V$. It should be noted that, in this case, $I_{DS} = 40\,mA$ because a single circuit will bias both transistors, so one had to design it for delivering twice the current necessary for each one.

The $\lambda/4$ transmission lines' physical dimensions were obtained (in *mils*[1]) using the *LineCalc* tool from ADS™ and considering an operating frequency of 3.432 GHz (UWB signal's central frequency), 90º of electrical length and an impedance which corresponds to approximately 99 Ω.

The values for the rest of the components - namely the capacitors C_1, C_2, C_4 and C_5 - were obtained by tuning, utilizing the lowest possible values that did not compromise the system's performance.

V_1 and V_2 components represent simple vias which connect the top side of the substrate to its bottom side.

4.5 VCSEL Biasing Network Design

The VCSEL also needs a biasing circuit in order to correctly set its working point. This biasing circuit will not only allow for the diode laser to work above the threshold current, it will also be responsible for setting the RIN current (as seen in eq. 2.9), thus contributing to its overall performance. Therefore, the DC current value which will be injected by this biasing network needs to be carefully chosen in order to obtain good results - in this case, a bias current of $I_b = 6\,mA$ has been found to be a sufficiently good bias point.

The bias network used to deliver this current in represented in figure 4.4, which also indicates its relative position in the transmitter. This bias network is comprised of a 5 V power source, a resistor R_b for setting up the DC current, an inductor L_b

[1]mil = thousandth of an inch or $2.54 \times 10^{-5}\,m$

for preventing the leakage of the UWB signals through this circuit and a capacitor C_b for DC-coupling.

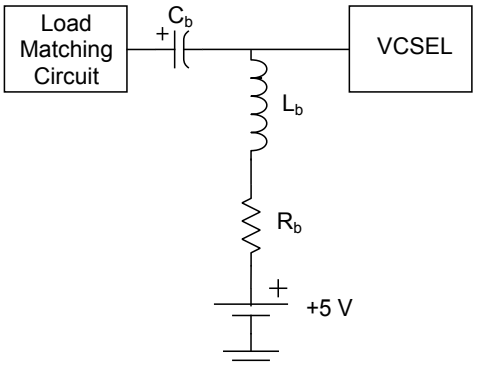

Figure 4.4: Biasing network for the VCSEL.

The values of the components are indicated in table 4.2. The value for the resistor R_b has been obtained by simply using the Ohm's Law ($V_b = 5\ V$), with the total resistance being the sum of R_b with $R_S = 76\,\Omega$ (subsection 2.4.2), this way ensuring that the current which is really being fed into the ILD is 6 mA,

$$R_b = \frac{V_b}{I_b} - R_S \tag{4.4}$$

Table 4.2: Values of the components of the VCSEL biasing network.

Component	Value	Unit
R_b	757	Ω
L_b	40	nH
C_b	10	pF

The values of the components C_b and L_b have been obtained by tuning since their purpose is filtering, but guaranteeing that the LNA is not significantly affected from the desired behavior, that is, guaranteeing they only filter the DC and the signal components, respectively. The effects of these electrical components together with the ones which compose the electrical circuit model for the VCSEL (see subsection 2.4.2) are depicted in figure 4.5, as well as the cutoff frequencies. It can be seen that the attenuation at the operating frequencies is negligible.

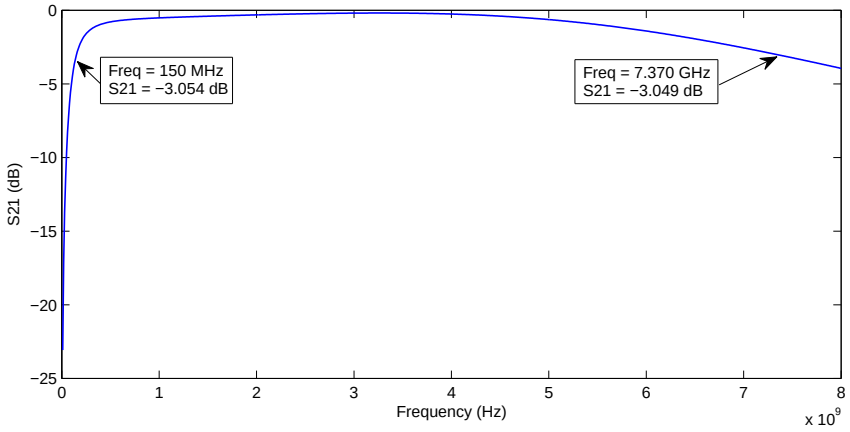

Figure 4.5: Frequency response of the VCSEL biasing circuit and parasitics.

4.6 Design of the Impedance Matching Circuits

Since the LNA is comprised of two transistors each one will need its own source and load matching circuits. Thus, there will be four matching circuits, based on the one represented in figure 4.6. Despite the open-circuit stubs being easier to fabricate, one had to use short-circuited stubs to facilitate the simulations and avoid convergence errors.

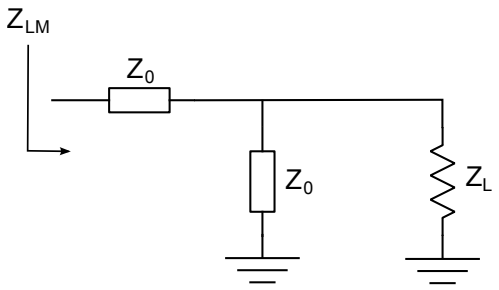

Figure 4.6: Schematic representation of an implemented matching network using a short-circuited stub.

These matching circuits were designed also with the aid of the *LineCalc* tool and the Smith chart from ADS™. Furthermore, they were designed for 4 GHz and considering a characteristic load impedance of 50 Ω, except for the last transistor, where its load matching circuit was designed considering it is loaded by the equivalent input impedance Z_{eq} of the VCSEL (subsection 2.4.2) together with the biasing circuit for the VCSEL (previous section). This biasing circuit should only contribute with the capacitor C_b for the overall load, since the rest is supposed to be an open-circuit

for the signals. The final result for the load impedance of the second transistor is then Z_{match}:

$$Z_{match} = Z_{eq} - \frac{j}{\omega C_b}$$

$$= \frac{R_S}{1 + R_S^2 C_P^2 \omega^2} + j\left(\omega L_P - \frac{1}{\omega C_b} - \frac{\omega R_S^2 C_P}{1 + R_S^2 C_P^2 \omega^2}\right) \tag{4.5}$$

which becomes $Z_{match} = 48.9 + j16.8$ at 4 GHz.

The Z_{LM} impedance represented in the figure is the required matched load impedance, that is, it is the value of the impedance one wishes to obtain after introducing the matching networks. It corresponds to the desired value of the reflection coefficient, using the following expression

$$Z_{LM} = \frac{Z_0 + \Gamma Z_0}{1 - \Gamma} \tag{4.6}$$

where $Z_0 = 50\,\Omega$ and $\Gamma = \Gamma_{S/L}$ which, in this case, corresponds to $\Gamma = S_{11}^*$ or $\Gamma = S_{22}^*$ for maximum unilateral gain.

After all of the transmission lines' dimensions were obtained, a simplification has been performed. This simplification is schematically explained in figure 4.7, where the load matching network of the first transistor and the source matching network of the second transistor were simplified by summing the admitances of the short-circuited stubs, so that only one short-circuited stub is used.

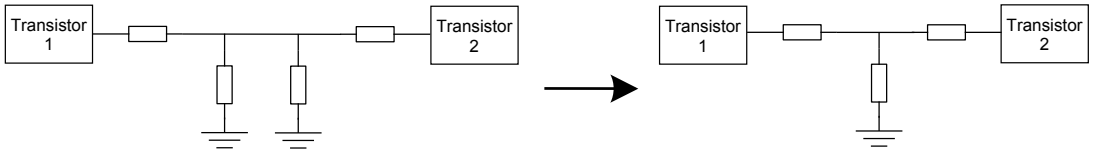

Figure 4.7: Simplification made to the matching networks between the first and the second transistor.

Moreover, some fine tuning has been made to two of the lines in these matching networks to attain a better frequency response. The final result, however, was not much different from the original, whether that be in the case of the lines' dimensions (given in table 4.3) or in the case of the final frequency response of the LNA.

Table 4.3: Dimensions of the transmission lines (TL) and stubs (S) used in the matching networks 1, 2 and 3 of figure 4.1. For example, the length of the first line of the matching network 2, $TL_{2,1}$, is 143.5 mil.

Component	Value	Unit
Length		
TL_1	134.5	mil
S_1	694.7	mil
$TL_{2,1}$	143.5	mil
S_2	576.5	mil
$TL_{2,2}$	134.5	mil
TL_3	71.7	mil
S_3	370.6	mil
Width		
All	43.2	mil

4.7 MOS Process

The MOS process to be used in the integration is an IBM 130 nm. The choice of this process was based on its proposed characteristics, like the material's response times, which is of absolute importance when considering a device that needs to work in the gigahertz range. These response times allow for a transition frequency that is above the frequency range the transistor is supposed to operate on. Other advantages of this process when compared to others that use different feature sizes is the fact that, with this one, one can produce a transmitter with smaller components and, hence, with lower power consumption and smaller intrinsic effects.

This process allows the use of five to eight different metal levels with different thicknesses. The metallization is made with copper or aluminum, depending on the level being considered – for example, the last level is usually made with copper. Isolation between devices is achieved with a shallow trench [27], which is a feature that creates trench patterns in the silicon and then fills them up with one or more dielectric layers, this way minimizing leakage currents.

4.8 Design of the IC Transmitter

As already explained in the previous chapter, every transmission line which has been used in the discrete version no longer exists because there are no propagation effects. This means that the $\lambda/4$ transmission lines in the biasing networks were replaced by inductors. Also, impedance matching is no longer achieved using transmission lines

but with lumped elements, as already discussed. The inductors were considered to present a quality factor (Q factor) whose chosen value differs whether they are inside the IC itself ($Q = 5$) or outside of it ($Q = 50$).

The first topic addressed was designing two transistors for the desired gain, that is, the same as the discrete version if possible. Starting from the signal current amplitude desired to feed the VCSEL - which is 1.2 mA considering the output resistance "seen" by the last transistor - the I_{DS} current could be defined, this way making it possible to calculate the corresponding transistor's transconductance, gain and physical dimensions by using the expressions presented in the previous subsection. The dimensions were found by also taking into consideration the transition frequency (F_T) of the transistor. The real biasing conditions for this transistor were simulated and found to be $V_{GSef} = 70\,mV$ and $I_{DS} = 3.9\,mA$, implying a transconductance of $g_m = 0.11\,\frac{A}{V}$. The first transistor has the same size and also presents the same biasing conditions as the last one. Furthermore, it has been found that both of them, besides having the same dimensions ($W = 118\,\mu m$ and $L = 130\,nm$), also present similar gains. As an example, the power gain of the last transistor was estimated to be around 17 dB.

As far as the biasing network is concerned, the same kind of circuit as represented in figure 4.3 is used, once again employing one for both transistors in order to minimize complexity. Also, some of its components, namely the resistors R_3, R_4 and R_5, have been altered to attend to the fact that the highest power supply voltage allowed for this technology is 3.3 V [27] and also for meeting the new biasing specifications. The values of the components used are indicated in table 4.4.

Table 4.4: Values of the components of the IC biasing network.

Component	Value	Unit
C_2	10	pF
C_3	0.1	μF
C_5	10	pF
C_6	0.1	μF
R_1	10	kΩ
R_2	10	kΩ
R_3	910	Ω
R_4	5090	Ω
R_5	60	Ω

The VCSEL biasing network is also the same as before (providing the same 6 mA bias current), but once again the values of its components are different due to the

change in the power supply voltage and due to the fact that this circuit will also affect the output impedance of the last transistor, this way changing its gain conditions. The new values of the components of the VCSEL biasing network are presented in table 4.5.

Table 4.5: Values of the electrical components used for the VCSEL biasing network in the IC.

Component	Value	Unit
R_b	474	Ω
L_b	20	nH

As already mentioned, the bondpads and bonding wires existent in every IC may also alter its behavior, making it necessary to consider them in the simulations for better assessing the final device behavior. Their simple electrical model has already been presented in figure 3.7: it is comprised of a parallel capacitor (representing the pad) and a series inductor (representing the bonding wire). The bonding wire's inductance ($L_{bonding}$) was considered to be 1 nH and the bondpad's capacitance (C_{pad}) was found to be 17 fF for a 73 μm x 73 μm pad [28].

Impedance matching to a 50 Ω source at the input and to the VCSEL equivalent impedance at the output of the circuit was made according to the models detailed in subsection 3.3.1, but as already said these models do not take into account many important elements which affect the input impedance (even the inductors of the biasing networks considerably affect it). This way, tuning has been made to the values of the components given by the models in order to obtain an acceptable matching, but the overall scheme presented in figure 3.6 has been maintained. The VCSEL model considered for the output impedance matching is the same as presented in subsection 2.4.2.

4.9 Summary

In this chapter the techniques for designing RF amplifiers have been put to use, allowing one to obtain the desired devices and to assess their properties.

Specifically for the discrete version of the transmitter, one has found that its LNA is potentially unstable at the operating frequencies, although being still possible to obtain maximum unilateral gain from it by designing the matching circuits to have $\Gamma_S = S_{11}^*$ and $\Gamma_L = S_{22}^*$. This gain has been found to be 16.1 dB for each transistor and, therefore, 32.2 dB for the system of two cascaded transistors which make the

LNA. With this gain being calculated assuming that it presents a unilateral behavior, the error to the actual obtainable gain has been estimated to be within 1.7 dB. Also, the noise figure for the whole ensemble was found to be 0.98 dB, a low value as desired.

Both biasing networks needed for the transmitter have been presented. These include the biasing network for both transistors, yielding voltages and currents in the transistors close to $V_{DS} = 3V$ and $I_{DS} = 20\,mA$ for them to work properly, and also having components which serve as filters and impedance matching networks to deliver some desirable features. The other biasing network detailed is the one used for VCSEL set up, a much simpler network which delivers 6 mA for the ILD while avoiding the leakage of the UWB signals.

The impedance matching circuits designed to obtain the needed reflection coefficients have also been presented, explaining how they were designed to match standard impedance values of 50 Ω or the equivalent load of the second transistor to each transistor's input and output impedances.

Then, the MOS process used was presented, as well as the design of the IC transmitter, which presents the same type of biasing networks as its discrete counterpart. In here, two transistors were designed, both with the same physical dimensions, $W = 118\,\mu m$ and $L = 130\,nm$, and estimated similar gains (17 dB).

The introduction in the schematic of bondpads (17 fF equivalent capacitance) and bonding wires (1 nH equivalent inductance) is desired for more realistic simulations due to their not-so-negligible effects on the overall system performance.

All the properties calculated in this chapter, related to the discrete or to the IC amplifier, will be compared in the next chapter to the simulations results when they are presented and discussed.

Chapter 5

Implementation and Simulation of the Optical Transmitter

5.1 Introduction

This chapter deals with the implementation of the transmitter and its simulations, whether they be relative to the discrete circuit or to the IC. All the simulations presented in this chapter were made using one of a set of three different EDA (Electronic Design Automation) softwares: ADS™ 2009, Matlab™ R2010a and Cadence™ v6.1. Sometimes both ADS™ and Matlab™ were used, such as in the case of Error Vector Magnitude (EVM) simulations. Although some simulations of the discrete transmitter carried out with ADS™ may refer to the same property as other simulations related to the IC version made with Cadence™, all of them are of extreme importance because they consider different properties that each version presents, since the designing conditions, technologies and propagation means are different. Therefore, some of these simulations made with different circuits may yield somewhat different results.

After this first introduction, the chapter continues by presenting the implementation results of the circuits and components discussed in chapter 4, by showing the schematics created using ADS™. The following section presents and discusses several simulation results of the properties of the discrete LNA, such as the S-parameters, noise figure, non-linear distortions and EVM measurements for the whole transmitting system.

Then, the results of the integration stage are presented, showing the circuit used to run the simulations in Cadence™. These simulation results are presented and discussed afterwards and also include the circuit's S-parameters, noise figure and non-linear distortions.

The layout of said circuit is then presented, explaining the options that have been considered so that the final result may resemble the most to the simulated circuit.

The chapter ends with a summary of the results obtained.

5.2 Implementation in ADS™

After all the design steps of the various components which compose the transmitter were performed (as presented in chapter 4), their actual implementation in ADS™ has been made to run the simulations. The result is shown in figure 5.1, which also includes the VCSEL biasing network (inside the red box).

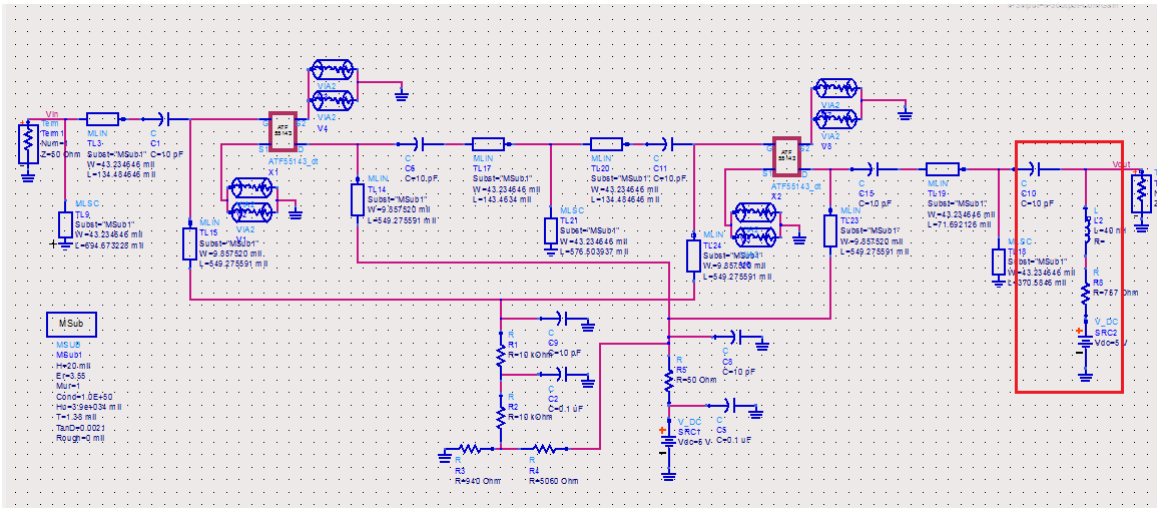

Figure 5.1: Schematic of the LNA and the VCSEL biasing circuit in ADS™.

This figure shows all the discussed elements of the transmitter (excluding the VCSEL itself), including the transistors models, both biasing networks and the matching circuits, as well as the components values (in the case of lumped components) and the physical dimensions (in the case of the transmission lines). It should be noted that these dimensions were calculated in *mils* just like in the case of the $\lambda/4$ lines, in accordance to the units used in the transistor model provided by its supplier. This model includes the parasitic elements of the transistor package and noise generation within itself, besides the typical description of the NFET's (N-type Field Effect Transistor) features needed for the simulations.

The UWB signal source used in this software is a predefined block where the signal parameters chosen are given in table 5.1. Time Frequency Code (TFC) 5 means there is no frequency hopping between sub-bands in the band group [4]. Furthermore, the

simulations have been made using a single data frame which in this particular case corresponds to 18.75 μs of simulation time.

Table 5.1: UWB signal parameters chosen for simulation purposes.

Parameter	Value/Type	Unit
Carrier Frequency	3.432	GHz
Data Rate	200	Mb/s
Modulation	QPSK	-
Band Group	1	-
Time Frequency Code	5	-

5.3 ADS™ Simulation Results

5.3.1 S-Parameters

Some of the S-parameters of the LNA have been obtained in the simulation, namely the magnitude and phase of S_{21} (gain) and S_{11}(reflection coefficient) parameters. These results are shown in figures 5.2a, 5.2b and 5.2c, respectively.

From the figure 5.2a one can almost immediately see that the gain is quite constant in the band of the UWB signal, an important characteristic needed to allow for similar amplifier response to the whole signal. Moreover, at 4 GHz the value of the gain is 30.7 dB, and 31 dB at a frequency close to the signal's central one (3.432 GHz). The gain at 4 GHz is less than the theoretically calculated value, which is 32.2 dB. This might have several reasons, starting with the fact that one has designed this LNA using a unilateral approach which yields an error for the value of each transistor's gain one actually obtains (refer to subsection 4.3.2), implicating an overall error for the cascaded transistor system. Despite this being the reason that might contribute the most for the mismatch between gain values, other factors might intervene, such as: a slight mismatch of the matching circuits at this frequency, because the fine tuning was performed to increase the gain at the signal's frequencies; and the fact that the $\lambda/4$ transmission lines used in the biasing network have been designed for the signal's central frequency and not for 4 GHz, to work properly at the actual operating frequencies. Concerning this last choice, it has been observed that if one had used 4 GHz the gain at this frequency would become 31.1 dB, a slightly higher value than the original one; however, at 3.432 GHz the gain would diminish, this way deteriorating the transmitter's gain at the operating frequencies of interest.

The phase of the S_{21} parameter (figure 5.2b) shows a fairly linear behavior which translates into approximately the same delay at all operating frequencies, particularly in the UWB signal's band, indicating that the distortion generation within the device might be fairly low.

As far as the S_{11} parameter (figure 5.2c) is concerned, we can see that its magnitude ranges between -4.8 dB and -7.1 dB inside the signal's band, which are relatively high values, with a minimum value of approximately -11.6 dB at 4 GHz. This implies that if the maximum allowed power for a wireless UWB signal is inserted into this amplifier (considering an antenna with unit gain), which is approximately -14.07 dBm or 40 µW [4], the value that will be sent back to the antenna will not exceed 14 µW. As this will hardly ever be the case, because this transmitter will always be at some distance from the UWB signal source, the actual reflected power will be much less than this value.

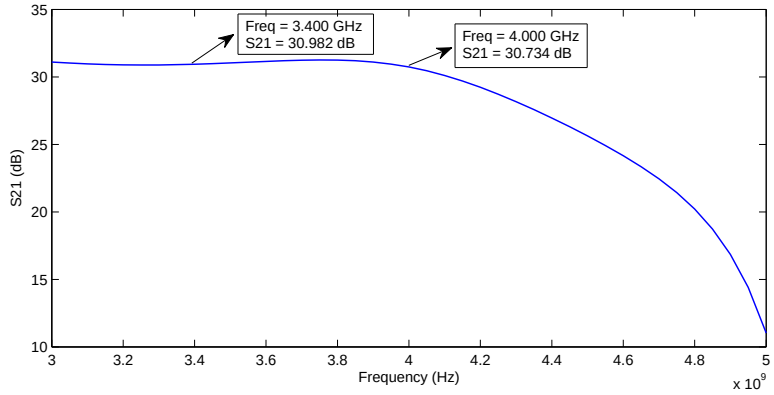

(a) Magnitude of the S_{21} parameter.

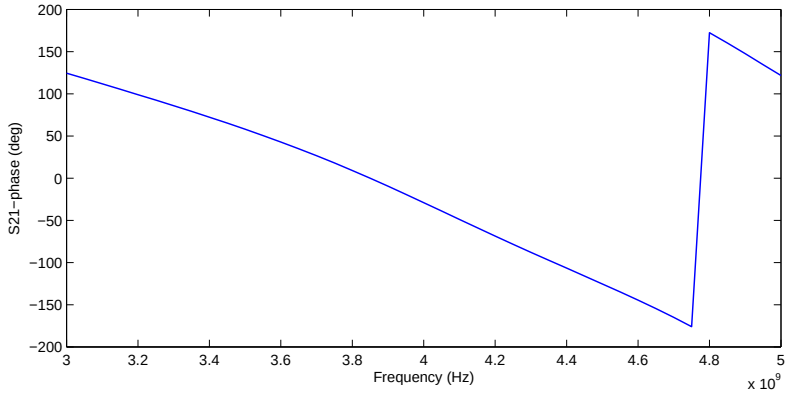

(b) Phase of the S_{21} parameter.

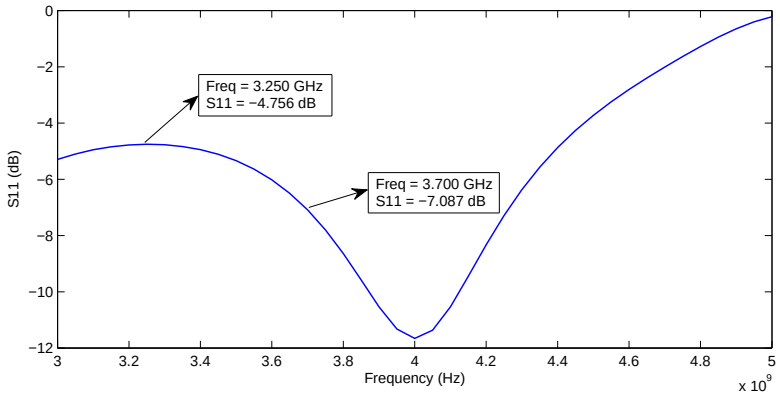

(c) Magnitude of the S_{11} parameter.

Figure 5.2: Magnitude and phase of the S_{21} and S_{11} parameters of the LNA.

5.3.2 Noise Figure

The noise figure for a wide range of frequencies has been simulated, giving the results shown in figure 5.3. At 3.9 GHz, which has been previously estimated to present

a 1 dB noise figure, it actually presents a slightly higher value (1.23 dB), probably due to the fact that the gain is lower than expected, as concluded in the previous subsection; also, other noise sources besides the two transistors considered in the calculations might be present.

It can also be seen that the top value at the signal frequencies is 1.02 dB, a low value as expected.

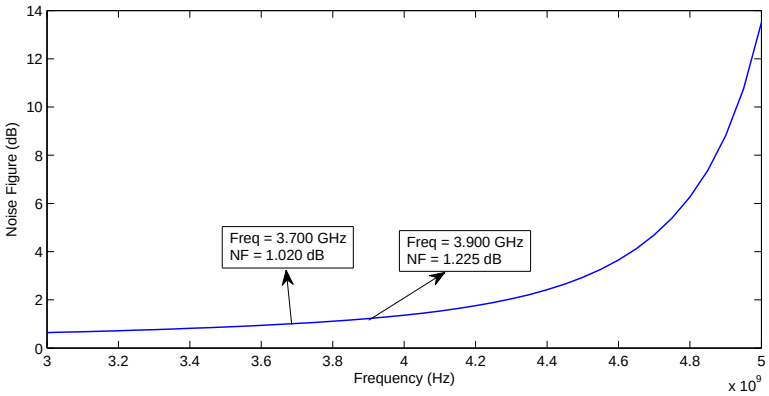

Figure 5.3: Simulated noise figure of the LNA.

5.3.3 Non-Linear Distortion

Non-linear distortion effects in this kind of devices are critical, particularly in OFDM-UWB applications where the signal is known to have a large peak-to-average power ratio. So their study is of extreme importance in order to assess *a priori* whether the transmitter's distortion effects will be negligible or, otherwise, will considerably influence its performance and decrease the reliability of the link and data quality.

In this way, some of the distortion parameters for the LNA have been simulated and are presented in table 5.2. These are the intermodulation distortion (IMD) parameters, specifically the input (IIP3) and output (OIP3) third-order intercept points and the Spurious-Free Dynamic Range (SFDR).

Table 5.2: Third-order intercept points and SFDR of the transmitter.

Third-order Intercept Points		
Parameter	Value	Unit
IIP3	-4.740	dBm
OIP3	27.085	dBm
SFDR	112.724	$\text{dB} \times \text{Hz}^{\frac{2}{3}}$

Other distortion studies have been made, namely based on the 1dB compression point, which is just another way of describing when the distortion effects in the LNA will become significant. Figure 5.4 represents the input-to-output power characteristics of the amplifier, where the red line represents the linear behavior for the fundamental frequency component and the blue line its compression curve. At the 1 dB compression point - where the compression curve deviates by 1 dB from the linear line - the input and output signal powers are indicated in table 5.3.

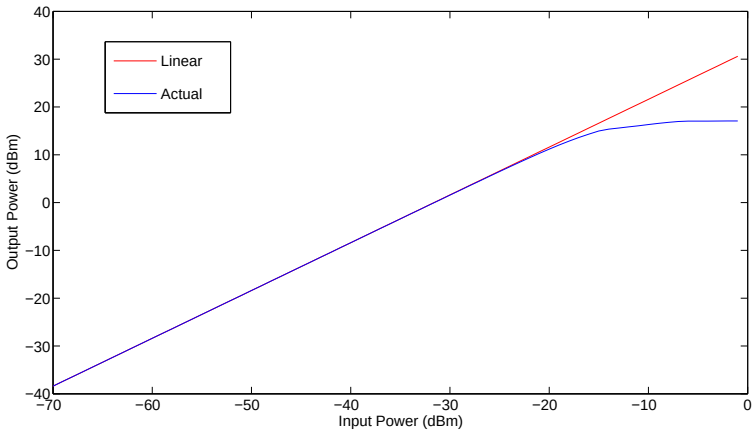

Figure 5.4: Linear (red) and compression curve (blue) of the LNA.

Table 5.3: 1 dB compression points.

1 dB Compression Points		
Parameter	Value	Unit
Input-referred	−15.66	dBm
Output-referred	13.92	dBm

In this way, for the maximum allowed input power of -14.07 dBm (for a signal with a 528 MHz bandwidth) the amplifier is operating at approximately 1.6 dB above the 1 dB compression point and 9.3 dB far from the IIP3. Thus, IMD spurious are only 18.6 dB below the fundamental (see appendix A), and the distortion impairment is already significant. In real operating conditions, however, where the UWB signal would travel through the wireless channel before reaching the transmitter, the signal level would be much lower than this and no intermodulation due to the amplifier is expected.

For instance, for a 1 meter wireless link the attenuation would be approximately 43.2 dB (refer to appendix B) and in this case the IMD spurious at the output of the amplifier would be approximately 100 dB below the fundamental. As yet another example, the UWB signal spectrum after leaving the source for an input power of -30 dBm (approximately 14 cm distance) is shown in figure 5.5a, and the spectrum of the same signal after passing through the LNA is shown in Figure 5.5b. It can be seen that both spectra are quite similar because third-order intermodulation distortion components are almost inexistent.

The impact of the VCSEL's nonlinear distortion on the UWB signal can be seen by comparing the power spectrum of this signal before (figure 5.5b) and after the VCSEL (figure 5.5c), where distortion effects are now much more visible at frequencies near the UWB signal, corresponding to third-order intermodulation distortion components.

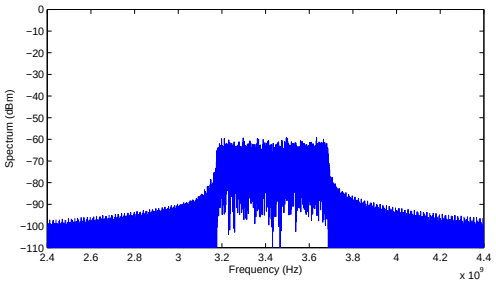

(a) UWB signal source spectrum.

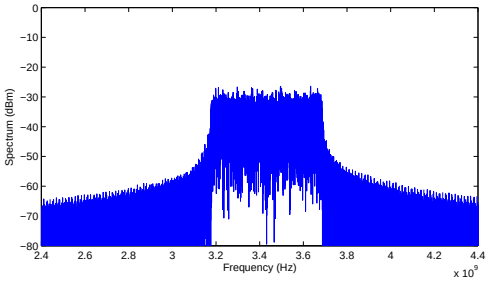

(b) UWB signal spectrum after passing through the LNA.

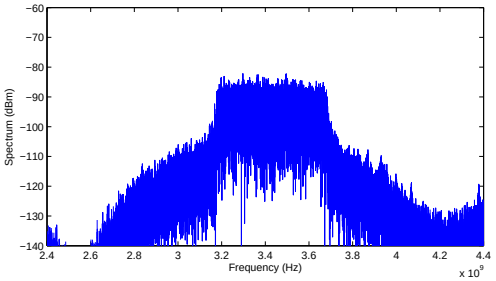

(c) UWB signal spectrum after passing through the LNA and the VCSEL.

Figure 5.5: UWB signal spectra after several transmission stages for an input power of -30 dBm.

5.3.4 Error Vector Magnitude (EVM)

In order to fully assess the performance of the whole transmitter, EVM simulations have been made by means of ADS™ and Matlab™ co-simulations, as already mentioned. A block diagram of the setup used for these co-simulations is depicted in

figure 5.6. ADS™ has been used to provide the UWB signal and simulate the electrical components effects, including the LNA and the VCSEL's parasitic components and bias network, whereas Matlab™ has been used to simulate the dynamic behavior of the ILD by solving the rate equations 2.1 and 2.2.

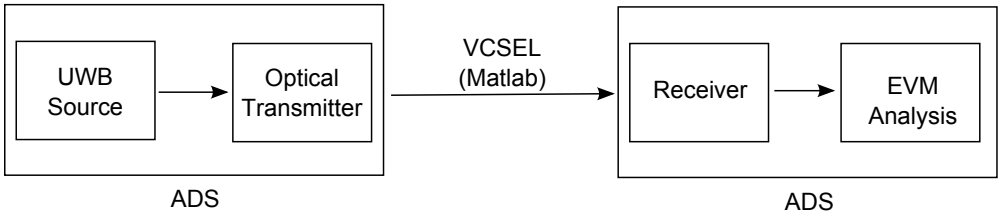

Figure 5.6: Simulation setup used for the EVM simulations.

Besides the simulation of this dynamic behavior, RIN has been added to provide for more realistic VCSEL performance results (refer to subsection 2.4.4). In this way, a RIN value of -150 dB/Hz has been chosen, based on RIN measurements made by INESC-TEC staff with off-the-shelf laser diodes. With this value, eq. 2.9 can be used to obtain the standard deviation of the RIN power if a responsivity value of $r = 1\,\frac{A}{W}$ is chosen. By multiplying a standard normal distribution with this power value and summing it with the VCSEL output power given by solving the rate equations, an additive white Gaussian noise approach has been made to model the RIN in the VCSEL.

Considering all these features of the VCSEL behavior, figure 5.7 represents the EVM data taken from the whole transmitting system at various amplifier input signal powers. It can clearly be seen a minimum EVM value for an input power of approximately -51 dBm. Below this value, the EVM deteriorates due to RIN becoming dominant; above this point, the EVM also increases, but mainly due to the nonlinear behavior of the VCSEL, given the low distortion generated by the amplifier as already discussed. Refer to figures 5.5b, whose EVM value corresponds to -40.2 dB, and 5.5c, whose EVM value corresponds to -14.9 dB, once again showing that the VCSEL is the main reason for signal distortion. Figures 5.8a, 5.8b and 5.8c present the constellation diagrams of the QPSK signal modulation scheme at different input powers (lowest, highest and best EVM input signal powers of figure 5.7), for better visualization purposes. It can be seen that, as expected, the diagram of the -51 dBm input signal power presents the best constellation, with the symbols being located closest to each other - hence the lowest EVM value.

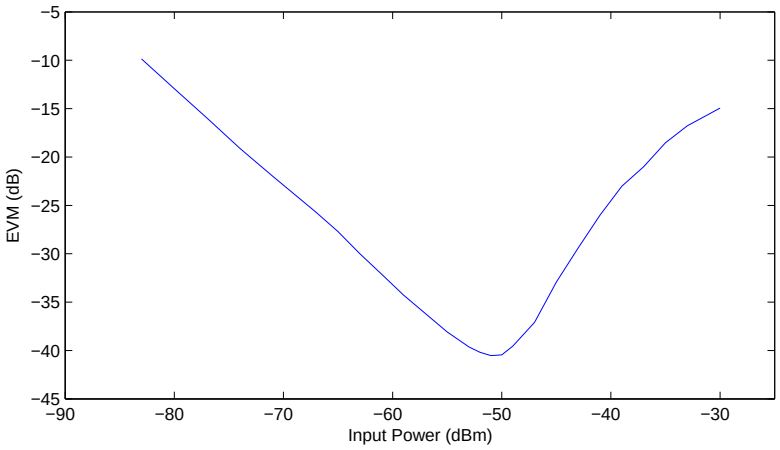

Figure 5.7: Transmitter EVM results for different input power values.

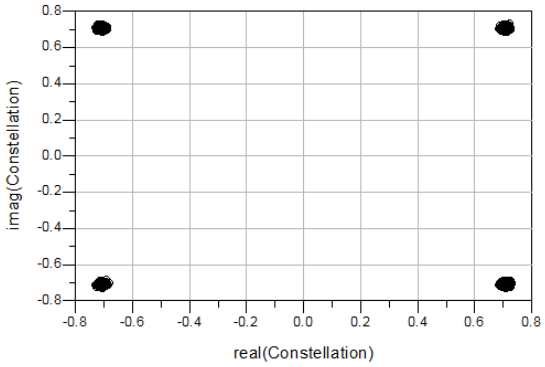

(a) Constellation diagram for an input signal power of -51 dBm.

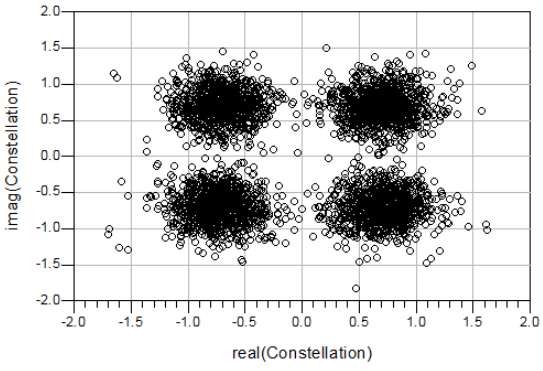

(b) Constellation diagram for an input signal power of -83 dBm.

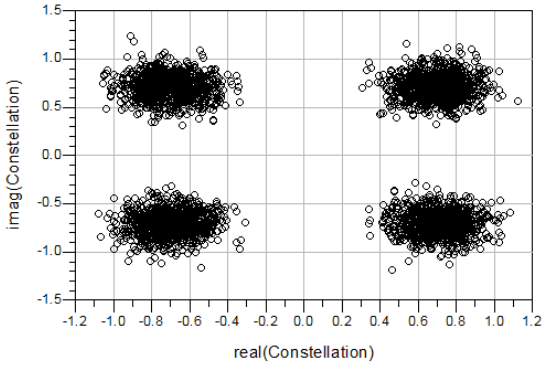

(c) Constellation diagram for an input signal power of -30 dBm.

Figure 5.8: Constellation diagrams of the UWB signal after passing through the optical transmitter, using different input powers.

If we consider an EVM value of -10 dB [29] to be sufficient for reliable data

transmission, then this device would be RIN limited and the corresponding signal input power would be approximately -87 dBm (considering a 4 dB gain for a typical UWB antenna), which corresponds to a maximum wireless distance of 31 meters. This was obtained considering that the signal is emitted in its maximum allowed power and the free-space path loss of a radio signal (appendix B), with the signal frequency considered being the central one.

Other important noise sources have not been considered in these studies and, therefore, in this maximum range estimation. These noise sources may include the channel and the antenna. Therefore, in real systems the true range will actually be lower.

5.4 Integration using the IBM 130 nm MOS Process with Cadence™

The result of the implementation techniques detailed in subsection 4.8 is presented in figure 5.9, showing the schematic created for the simulation studies to be made with Cadence™ and highlighting the VCSEL biasing network (red box) and a bondpad model (blue box) for easier visualization.

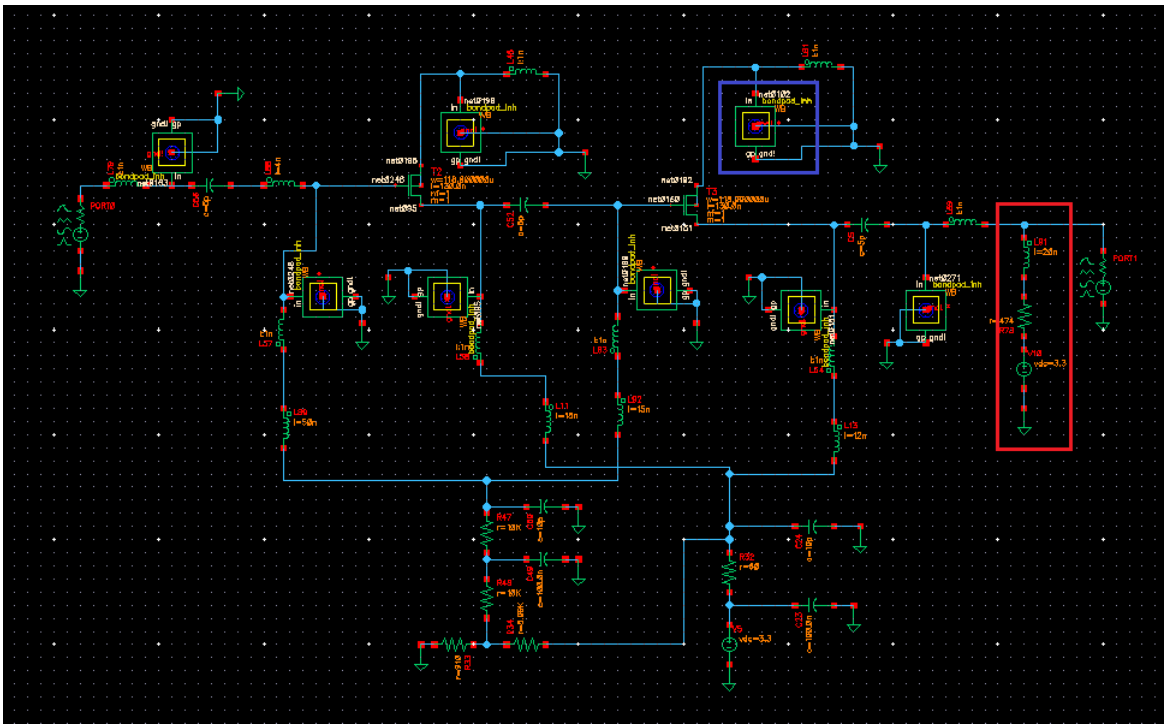

Figure 5.9: Schematic of the circuit used for simulations, made with Cadence™.

The model used for the transistors is a N-type FET provided by the technology library. The model used for the bondpads is also provided by the technology library (presenting a 17 fF capacitance) and the bonding wire is modeled by a 1 nH series inductor, which have been inserted in all the places of the circuit that will need to have outside connections (pins). The elements that are left inside the circuit area limited by the bondpads make the integrable circuit, which can only be composed of small components and the transistors in order to avoid creating a large IC.

As far as the input impedance matching components is concerned, a 5 pF capacitor (C_G) has been used together with a 4 nH series inductor (L_G), obtained by tuning. At the output, the DC-coupled capacitor C_{out} also has 5 pF, enough to obtain good impedance matching without severely attenuating the signals.

5.5 Cadence™ Simulation Results

5.5.1 S-Parameters

Just like it was done for the discrete LNA, the main S-parameters of the circuit designed with Cadence™ have also been obtained.

It can be seen from figure 5.10a that the gain of the amplifier is not flat, being a maximum 31.1 dB in the lower operating frequencies and decreasing until 29.1 dB at the top frequency limit. Despite this meaning a 2 dB difference between gains in the operating signal range, it is still below the 3 dB limit (cut-off frequency definition), making it acceptable. However, it is worse than the behavior obtained in the case with discrete components but, once again, the design conditions are quite different and a very similar behavior should not be expected.

From the S_{21} phase results (figure 5.10b), it can be seen that it does not present a very linear behavior and that it might, therefore, distort more the transmitting signal as it passes through the device than the other version.

As far as the S_{11} result is concerned, its magnitude is presented in figure 5.10c which indicates a quite small value for the top frequencies (-16.8 dB), whereas this increases as the frequency becomes smaller, ultimately yielding -3.1 dB for the lower frequency limit. This is a relatively large value, which might impose future stability problems. However, it has been found that the transmitter is unconditionally stable at these frequencies, having a stability factor of $K = 1.04$ and $\Delta = 0.79$. But the amount of reflected signal back to the antenna could become quite large if the input power approaches the maximum allowed – i.e., if this device is placed close to the emitting one.

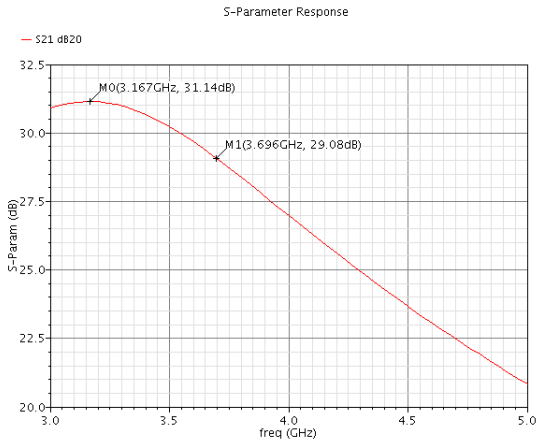

(a) Magnitude of the S_{21} parameter of the IC.

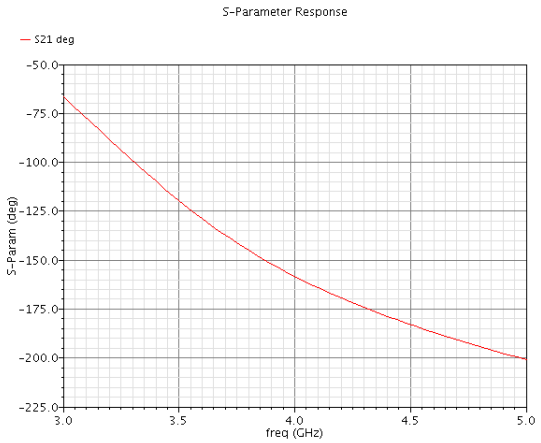

(b) Phase of the S_{21} parameter of the IC.

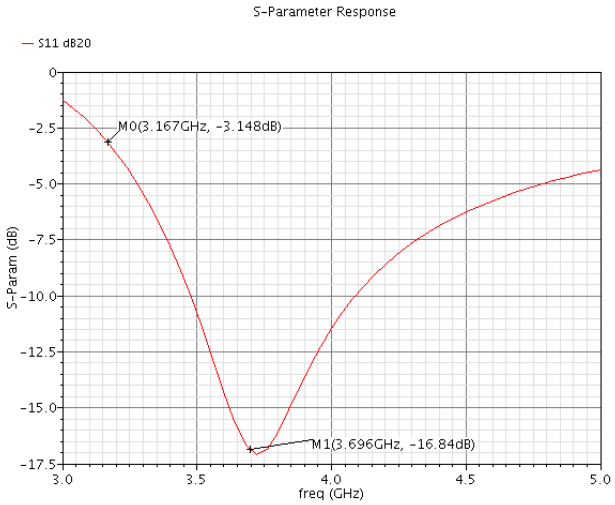

(c) Magnitude of the S_{11} parameter of the IC.

Figure 5.10: Magnitude and phase of the S_{21} parameter and magnitude of the S_{11} parameter of the circuit implemented with Cadence™.

5.5.2 Noise Figure

The noise figure has also been obtained and the result is depicted in figure 5.11. It is clear that these are worse results than the ones in the previous case, with the values being situated between 1.89-1.77 dB. Nevertheless, these are still very good results, with the increment relatively to the other case being possibly due to the use of inductors with a Q factor instead of the transmission lines, besides the difference in transistor technology and design.

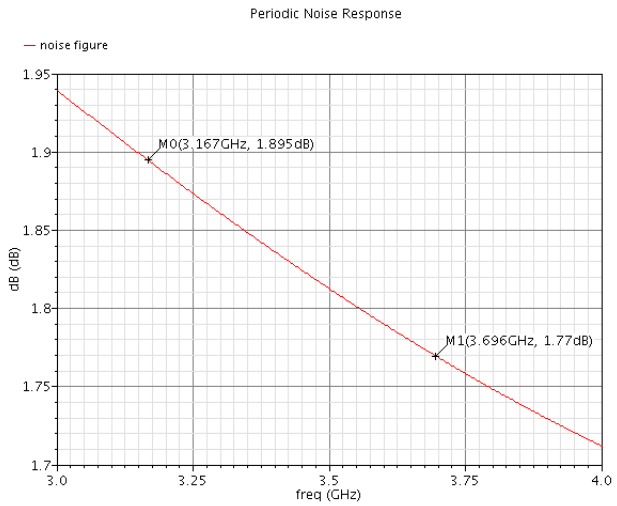

Figure 5.11: Noise figure of the LNA.

5.5.3 Non-Linear Distortion

Non-linear distortion studies have also been made for this implementation of the transmitter. Table 5.4 gives the IIP3 and OIP3 points for this circuit and we can see that they are smaller than the values for the discrete transmitter. This clearly indicates that the IC has a more non-linear behavior than the discrete version, thus decreasing the maximum input power allowed for obtaining a linear response - hence the lower IIP3. This value is even lower than the maximum power allowed by the UWB standard, once again meaning that it is not advised to use this transmitter in very short range applications (very small distances from the emitting antenna), where the input signal power is higher and the non-linear effects will be significant. But using the same example as before, after a one meter wireless link the IMD spurious would be approximately 85 dB below the fundamental one, a much better situation where the distortion effects are negligible. In principle, these distances will be the rule and not the exception and the transmitter response is expected to be considerably linear in typical applications.

Table 5.4: Input and output-referred third-order intercept points for the circuit implemented using Cadence™.

Third-Order Intercept Points		
Parameter	Values	Unit
IIP3	-14.4	dBm
OIP3	13.7	dBm

The compression curve is depicted in figure 5.12 and the input and output-referred 1 dB compression points are presented in table 5.5. These values are also lower than their discrete transmitter counterparts and the input-referred point is much lower than -14.07 dBm, showing that if the device is placed close to the emitting antenna the gain will not be the one presented in subsection 5.5.1, but lower because a compression (saturation) will happen. This is just one more indication that for short distances this transmitter is not a very good choice.

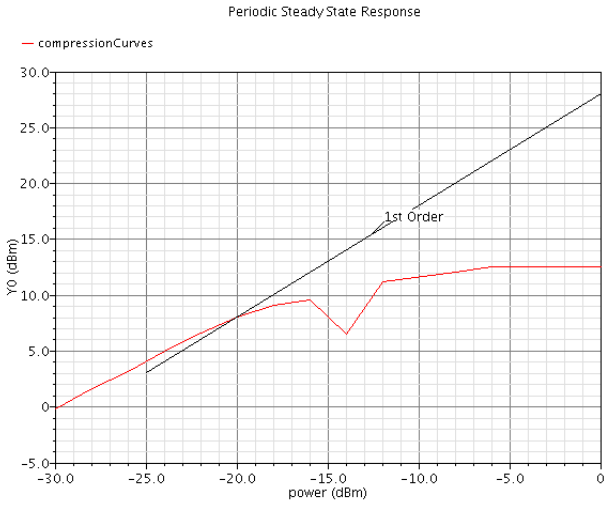

Figure 5.12: Compression curve and 1 dB compression point of the LNA.

Table 5.5: Input and output-referred 1 dB compression points for the circuit implemented using Cadence™.

1 dB Compression Points		
Parameter	Values	Unit
Input-referred	-19.97	dBm
Output-referred	8.09	dBm

5.6 Layout of the Integrated Circuit using Cadence™

As already mentioned, the only integrable components of this circuit are the ones inside the area limited by the bondpads: the components that make the input impedance matching, the DC-coupling capacitors and the two transistors; the others have been excluded from integration due to its large values, which would also mean a large layout size.

In this way, figure 5.13 presents the layout of these components making the IC device, together with the different metal connections between them and the eight bondpads needed for input-to-output (IO) connections, all of them arranged in a rectangular shape to facilitate further integration steps. It can be clearly seen from this picture the very large size of the 4 nH inductor when compared to the other components, occupying a 170 µm x 170 µm area of the 546 µm x 454 µm total layout area. This means that, for example, the other inductors in the circuit of figure 5.9 - which have inductance values several times larger than this one - would have even bigger dimensions making their integration impractical and unwanted, both due to the final chip size that would be obtained and to the larger intrinsic effects that would be created. This inductor model has specific layout rules because it needs to be separated from the other components by an appropriate distance, so that no efficient energy coupling exists and no losses are introduced.

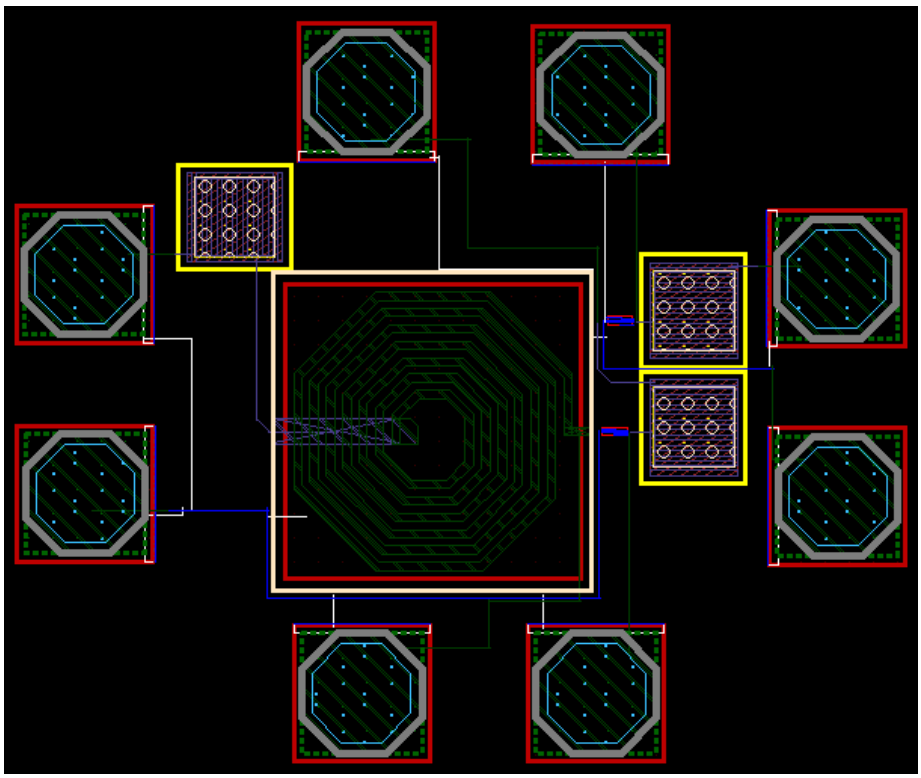

Figure 5.13: Layout of the components making the IC.

The transistors have been laid out using a stacked layout technique due to their large width/length ratio, which involves dividing the transistor into narrower ones and connecting them in the correct manner for optimum operation. This approach allows one to diminish losses and intrinsic capacitances, while providing a more friendly

rectangular shape for layout. An example of this technique employed in one of the transistors is depicted in figure 5.14, where the several resulting "fingers" and their connections can be seen.

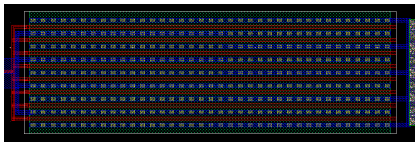

Figure 5.14: One of the transistors designed, where the stacked layout technique can be observed.

Several vias are used throughout this layout to provide a connection to different metal layers since, for example, the connections to the bondpads are made with the top metal layer. Also, substrate contacts were placed in every ground connection and near both transistors.

The metal lines connecting the IO bondpads to the circuit components were designed with the necessary width to withstand the currents, which means a width of about 1 µm for the DC currents used in this design. The rest of the connections, namely the ones making the UWB signal path, present the same width and were made as short as possible to avoid propagation effects.

Finally, the capacitor, inductor and bondpad layout models used were provided by the technology library. These come with groundplanes implemented in order to decrease intrinsic parasitic effects in the chip and whose connections to ground have also been made using the appropriate layer.

After adding the package and its connections (pins and bonding wires) the IC is completed, although this would mean taking several other design and verification steps before reaching this final stage (which have not been carried out in this work). The transmitter would be completed by inserting the rest of the components whose layout has not been made in a PCB that would connect them to the fabricated chip. Using state-of-the-art surface-mount technology (SMT), capable of delivering very small PCB components, the final device could become very small; these dimensions would only be limited by the other transmitter elements that are intrinsically larger - the UWB antenna and the necessary power source for powering the LNA and the VCSEL.

5.7 Summary

This chapter dealt with the implementation of the circuits and with the various simulation results obtained both with ADS™ and Cadence™, which gave a glimpse on how the different versions of the transmitter will behave if put to use in real conditions.

This being said, the discrete transmitter presents a stable gain around 31 dB throughout the entire UWB signal frequency range, although being a bit lower than its estimated gain. Its noise figure tops 1 dB at the maximum signal frequency, a very good value even when not considering the VCSEL noise in this result. The non-linear distortions caused by the circuit have been found not to be significant at real-life operating conditions, meaning this device will not affect severely the data being transmitted. However, when considering the VCSEL dynamic behavior in EVM simulations, one has found that the device presents an optimum input signal power (-51 dBm) at which the corresponding EVM value is a minimum and that this value is bounded by the ensemble's noise at lower powers and by the VCSEL distortion for higher input powers.

On the other hand, the IC version of the transmitter was first implemented and simulated as an analogue microelectronics circuit and considering some effects that only these circuits present, like the bondpads' and bonding wires' intrinsic behavior. The results show a circuit with overall results worse than the discrete version, specifically: the varying gain along the operating signal frequencies (going from 31.1 to 29.1 dB); the higher noise figure (around 1.8 dB) not considering the VCSEL RIN; and, the lower IIP3, OIP3 and 1 dB compression points resulting in higher distortion of the signals.

Its layout has then been made, taking into account all the necessary rules in order to avoid introducing into the chip even more unwanted intrinsic effects than the ones already considered. The layout yielded a low complexity and small size IC, whose layout measures just 546 µm x 454 µm. The final device size would only depend on the external components that are needed for this transmitter to work, like the power source and the antenna.

Chapter 6

Conclusion

The main goal of this thesis was to design and simulate an optical transmitter for UWB signals based on discrete COTS components and MOS technology. Considering their simulated properties and expected behavior under future possible applications, I believe this goal has been achieved.

The thesis itself presented several chapters before delivering the final results. Chapter 1 gave a short introduction to the entire work, briefly presenting its motivations and goals as well as somewhat similar projects recently developed by groups worldwide.

In chapter 2 the main features of the RoF systems have been presented, as well as some of the features of UWB signals. Moreover, the structure, properties and model used to simulate the VCSEL have also been explained, including the RIN these lasers usually present.

In chapter 3 the design techniques to obtain RF amplifiers have been explained, whereas in chapter 4 these have been applied to design both versions of the desired transmitter and to estimate some of their properties.

In chapter 5 their actual implementation and simulation using either ADS™ or Cadence™ has been performed, extracting the main properties for behavior assessment.

Specifically speaking about the final results, the discrete transmitter is a low complexity device with a high gain and very low noise figure, whose response in real applications can be considerably linear. This device has been simulated with a specific 200 Mb/s QPSK-modulated UWB signal and typical VCSEL parameters, giving a maximum estimated range of 31 meters and limited only by the VCSEL RIN, a value that is suitable for most of the desired applications. In reality this range will, however, be reduced due to the existence of other noise sources and wireless channel effects.

The IC proposed only includes some of the smaller elements and would, therefore, need to be integrated in a PCB with the rest of the transmitter components. It also yielded some satisfactory results, with a varying but still acceptable gain in the desired frequency band, a small noise figure and distortion effects that might not be of significant importance if short-range applications (where, for example, the MSs are very close to the BSs) are avoided. The layout of the integrable components resulted in a small and low complexity IC whose current consumption does not surpasses 8 mA, a small value when compared to the 40 mA (approximately) of the discrete version. The final transmitter device, including both the IC and PCB components, could also be of small dimension and, therefore, suitable for a wide range of RoF applications where small size BSs are desired and where this device would be inserted.

Finally, there are always some aspects that could be improved in future work, mainly in the IC case but also with regard to the general amplifying operation. Concerning the IC, a more stable gain at the operating frequency range could be sought, as well as a more linear response so that it can be used in shorter distances without it affecting its performance. Also, it should be studied if smaller electrical components might be utilized in order to integrate as many elements of the transmitter as possible and, therefore, decrease even more the final transmitter size. Regarding the amplification process, it could be used a gain control loop to change the gain depending on the input power, since in reality it will never be exactly the same at all times. This gain control loop could be designed to always feed the VCSEL the specific signal power that allows for optimum operation, as found out in the EVM simulations presented.

References

[1] H. B. Kim, "Radio over fiber based network architecture," Ph.D. dissertation, Technischen Universitat Berlin, October 2005.

[2] H. M. Salgado, J. M. B. Oliveira, and N. Lima, "Modelling optical/RF impairments in ultra-wideband radio over fiber," Photonic Components for Ultra-Wideband Radio over Optical Fiber (UROOF), Tech. Rep., 2008.

[3] D. Pozar, *Microwave Engineering*, , 3rd edition ed. Wiley, 2005.

[4] *Standard ECMA-368: High Rate UltraWideband PHY and MAC Standard, 3rd Edition*, ECMA International Std., December 2008.

[5] D. Porcino and W. Hirt, "Ultra-wideband radio technology: Potential and challenges ahead," *IEEE Communications Magazine*, July 2003.

[6] K. Siwiak, "Ultra-wide band radio: introducing a new technology," in *Vehicular Technology Conference, 2001. VTC 2001 Spring. IEEE VTS 53rd*, vol. 2. IEEE, 2001, pp. 1088–1093.

[7] T. Quinlan, M. Morant, S. Dudley, R. Llorente, and S. Walker, "480-Mbit/s UWB bi-directional radio over fiber CWDM PON using ultra-low cost and power VCSELs," *Optics Express*, vol. 19, no. 26, pp. B197–B202, 2011.

[8] D. Watanabe, A. Ono, and T. Okayasu, "CMOS optical 4-PAM VCSEL driver with modal-dispersion equalizer for 10-Gb/s 500m MMF transmission," in *Solid-State Circuits Conference-Digest of Technical Papers, 2009. ISSCC 2009. IEEE International*. IEEE, 2009, pp. 106–107.

[9] W. Oh and K. Park, "Design of a 4-channel 10-Gb/s CMOS VCSEL driver array," in *Optical Internet, 2008. COIN 2008. 7th International Conference on*. IEEE, 2008, pp. 1–2.

[10] S. Palermo and M. Horowitz, "High-speed transmitters in 90nm CMOS for high-density optical interconnects," *European Solid-State Circuits Conference*, pp. 508–511, 2006.

[11] M. Beltran, J. Jensen, X. Yu, R. Llorente, R. Rodes, M. Ortsiefer, C. Neumeyr, and I. Monroy, "Performance of a 60-GHz DCM-OFDM and BPSK-impulse ultra-wideband system with radio-over-fiber and wireless transmission employing a directly-modulated VCSEL," *Selected Areas in Communications, IEEE Journal on*, vol. 29, no. 6, pp. 1295 –1303, june 2011.

[12] D. Opatic and G. Croatia, "Radio over fiber technology for wireless access," *Ericsson Nikola Tesla dd, Krapinska*, vol. 45, 2009.

[13] A. Ngoma, "Radio-over-fibre technology for broadband wireless communication systems," Ph.D. dissertation, Technische Universiteit Eindhoven, 2005.

[14] C. Lim, A. Nirmalathas, M. Bakaul, P. Gamag, K.-L. Lee, D. N. Y. Yang, and R. Waterhouse, "Fiber-wireless networks and subsystem technologies," *Journal of Lightwave Technology*, vol. 28, pp. 390–405, 2010.

[15] http://www.rp-photonics.com (Encyclopedia of Laser Physics and Technology). (December 2011) Rp-photonics.

[16] K. Iga, "Surface-emitting laser: Its birth and generation of new optoelectronics field," *IEEE Journal on Selected Topics in Quantum Electronics*, vol. vol. 6, no. 6, November/December 2000.

[17] L. A. Coldren and S. W. Corzine, *Diode Lasers and Photonic Integrated Circuits*. John Wiley and Sons, Inc, 1999.

[18] C. Wilmsen, H. Temkin, and L. Coldren, *Vertical-Cavity Surface-Emitting Lasers: Design, Fabrication, Characterization, and Applications*. Cambridge University Press, 1999.

[19] M. Bruensteiner and G. C. Papen, "Extraction of VCSEL rate-equation parameters for low-bias system simulation," *IEEE J. of Selected Topics in Quantum Electronics*, vol. 5, pp. 487 – 494, 1999.

[20] H. M. Salgado, "Performance assessment of subcarrier multiplexed optical systems: Implications of laser nonlinearities," Ph.D. dissertation, School of Electronic Engineering and Computer Systems, University of Wales, Bangor, UK, November 1993.

[21] C. H. Cox III, *Analog Optical Links - Theory and Practice*. Cambridge University Press, 2004.

[22] H. M. Salgado, *Lectures of "Engenharia de RF e Microondas"*. Faculdade de Engenharia da Universidade do Porto, 2011.

[23] R. Gilmore and L. Besser, *Practical RF Circuit Design for Modern Wireless Systems: Active Circuits and Systems*. Artech House, Inc., 2003, vol. II.

[24] A. Sedra and K. Smith, *Microeletronic Circuits*, 4th ed. Oxford University Press, 1998.

[25] J. Machado da Silva, *Lectures of "Microelectrónica Analógica"*. Faculdade de Engenharia da Universidade do Porto, 2011.

[26] *Data Sheet: ATF-55143 - Low Noise Enhancement Mode Pseudomorphic HEMT in a Surface Mount Plastic Package*, Avago Technologies.

[27] I. M. Division, "Foundry technologies: 130-nm CMOS and RF CMOS," IBM, Tech. Rep., 2003.

[28] *IBM Foundry and Manufacturing Services Education: CMOS8RF(CMRF8SF) Design Kit Training V1.3.1.0*.

[29] L. Pessoa, D. Coelho, J. Oliveira, J. C. S. Castro, and H. M. Salgado, "Experimental evaluation of R-EAM performance in RoF networks," in *International Symposium on Green Radio over Fibre & All Optical Technologies for Wireless Access Networks*, June 2011.

[30] A. B. Carlson and P. B. Crilly, *Communication Systems: An Introduction to Signals and Noise in Electrical Communication*, 5th ed. McGraw-Hill, 2010.

Appendix A

Power Relation Between Spurious and Fundamental Components Through Intermodulation Distortion

In figure A.1 is represented the input-to-output power characteristics of a generic non-linear system.

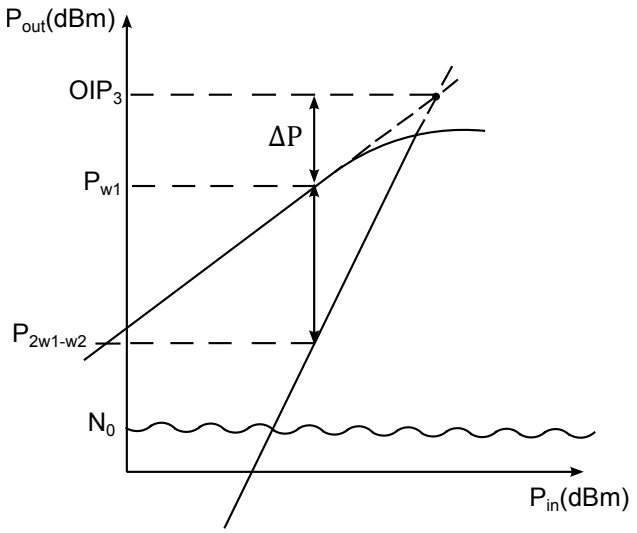

Figure A.1: Input-to-output power characteristics of a non-linear system.

In order to find out the relative power of the spurious when compared to the fundamental frequency component, assuming this fundamental component's power is still in the linear region, one must first know the relation between their linear power characteristics [22],

$$P_{2\omega_1-\omega_2} = 3P_{\omega_1} - 2P_3 \tag{A.1}$$

From figure A.1 it is easy to relate P_{ω_1} to the output third-order interception point OIP3

$$P_{\omega_1} = P_3 - \Delta P \tag{A.2}$$

which by introducing in eq. A.1 yields

$$P_{2\omega_1-\omega_2} = 3P_3 - 3\Delta P - 2P_3$$

$$= P_3 - 3\Delta P$$

Using once more the eq. A.2 we obtain the desired relation between the powers of the frequency components

$$P_{\omega_1} - P_{2\omega_1-\omega_2} = 2\Delta P$$

Appendix B

Free-Space Path Loss

The Friis radio link formula addresses the issue of how much signal power is received at an isotropic antenna after being transmitted by another antenna and free-space propagated. This formula can be expressed as [3]

$$P_r = \frac{G_t G_r \lambda^2}{(4\pi l)^2} P_t \tag{B.1}$$

where P_r and P_t are the received and transmitted powers, respectively, G_t and G_r are the receiving and transmitting isotropic antenna gains, respectively, λ is the radio signal free-space wavelength and l is the distance between antennas. This formula does not include important and realistic phenomena which occur in every wireless propagation, like medium absorption, scattering and multipath effects, which would diminish the amount of power received. It only considers the losses and effective aperture areas of the antenna and signal power loss due to spherical dispersion of the energy with travelled distance.

If one takes eq. B.1 and consider both antenna gains to be unitary, $G_t = G_r = 1$, then one gets the free-space path loss (L) of a radio signal [30]

$$\begin{aligned} L = \frac{P_t}{P_r} &= \left(\frac{4\pi l}{\lambda}\right)^2 \\ &= \left(\frac{4\pi l f}{c}\right)^2 \end{aligned} \tag{B.2}$$

where f is the signal's frequency.

Eq. B.2 becomes

$$FSPL(dB) = 20log_{10}(l) + 20log_{10}(f) - 27.55$$

if expressed in dB, with l in meters and f in megahertz.